Galaxy halo masses and satellite fractions from galaxy–galaxy lensing in the Sloan Digital Sky Survey: stellar mass, luminosity, morphology and environment dependencies

Rachel Mandelbaum,[1]★ Uroš Seljak,[1,2] Guinevere Kauffmann,[3] Christopher M. Hirata[4] and Jonathan Brinkmann[5]

[1]*Department of Physics, Jadwin Hall, Princeton University, Princeton, NJ 08544, USA*
[2]*International Centre for Theoretical Physics, Strada Costiera 11, 34014 Trieste, Italy*
[3]*Max-Planck-Institut für Astrophysik, Karl-Schwarzschild-Strasse 1, 85748 Garching, Germany*
[4]*Institute for Advanced Study, Einstein Drive, Princeton, NJ 08540, USA*
[5]*Apache Point Observatory, 2001 Apache Point Road, Sunspot, NM 88349, USA*

ABSTRACT

The relationship between galaxies and dark matter (DM) can be characterized by the halo mass of the central galaxy and the fraction of galaxies that are satellites. Here, we present observational constraints from the Sloan Digital Sky Survey on these quantities as a function of r-band luminosity and stellar mass using galaxy–galaxy weak lensing, with a total of 351 507 lenses. We use stellar masses derived from spectroscopy and virial halo masses derived from weak gravitational lensing to determine the efficiency with which baryons in the halo of the central galaxy have been converted into stars. We find that an L_* galaxy with a stellar mass of $6 \times 10^{10} \, \mathrm{M_\odot}$ is hosted by a halo with mass of $1.4 \times 10^{12} \, h^{-1} \, \mathrm{M_\odot}$, independent of morphology, yielding baryon conversion efficiencies of 17^{+10}_{-5} per cent (early-types) and 16^{+15}_{-6} per cent (late-types) at the 95 per cent confidence level (statistical, not including systematic uncertainty due to assumption of a universal initial mass function). We find that for a given stellar mass, the halo mass is independent of morphology below $M_{\mathrm{stellar}} = 10^{11} \, \mathrm{M_\odot}$, in contrast to typically a factor of 2 difference in halo mass between ellipticals and spirals at a fixed luminosity. This suggests that stellar mass is a good proxy for halo mass in this range and should be used preferentially whenever a halo mass selected sample is needed. For higher stellar masses, the conversion efficiency is a declining function of stellar mass, and the differences in halo mass between early- and late-types become larger, reflecting the fact that most group and cluster haloes with masses above $10^{13} \, \mathrm{M_\odot}$ host ellipticals at the centre, while even the brightest central spirals are hosted by haloes of mass below $10^{13} \, \mathrm{M_\odot}$. We find that the fraction of spirals that are satellites is roughly 10–15 per cent independent of stellar mass or luminosity, while for ellipticals this fraction decreases with stellar mass from 50 per cent at $10^{10} \, \mathrm{M_\odot}$ to 10 per cent at $3 \times 10^{11} \, \mathrm{M_\odot}$ or 20 per cent at the maximum luminosity considered. We split the elliptical sample by local density, and find that at a given luminosity there is no difference in the signal on scales below $100 \, h^{-1}$ kpc between high- and low-density regions, suggesting that tidal stripping inside large haloes does not remove most of the DM from the early-type satellites. This result is dominated by haloes in the mass range 10^{13}–$10^{14} \, h^{-1} \, \mathrm{M_\odot}$, and is an average over all separations from the group or cluster centre.

Key words: gravitational lensing – galaxies: haloes – galaxies: stellar content.

1 INTRODUCTION

The connection between the spatial distribution of galaxies and dark matter (DM) is an essential ingredient in the physics of

★E-mail: rmandelb@princeton.edu

galaxy formation. One very useful probe of the galaxy–DM connection that recently became available is weak lensing around galaxies, or galaxy–galaxy (hereafter g–g) lensing (Tyson et al. 1984; Brainerd, Blandford & Smail 1996; Hudson et al. 1998; Fischer et al. 2000; McKay et al. 2001; Smith et al. 2001; Hoekstra et al. 2003; Hoekstra, Yee & Gladders 2004; Sheldon et al. 2004; Mandelbaum et al. 2005a; Seljak et al. 2005). Gravitational lensing induces tangential shear distortions of background galaxies around foreground galaxies, allowing direct measurement of the galaxy–DM correlation function around galaxies. The individual distortions are small (of order 0.1 per cent), but by averaging over all foreground galaxies within a given subsample, we obtain high signal-to-noise ratio (S/N) in the shear as a function of angular separation from the galaxy. If we know the lens redshifts, the shear signal can be related to the projected mass density as a function of proper distance from the galaxy. This allows us to determine the averaged DM distribution around any given galaxy sample.

In recent years, the progress on the observational side of g–g lensing has been remarkable. In the latest Sloan Digital Sky Survey (SDSS) analyses (Sheldon et al. 2004; Seljak et al. 2005), $20–30\sigma$ detections of the signal as a function of physical separation have been obtained. Similarly, high-S/N detections have also been observed as a function of angular separation with other surveys (Hoekstra et al. 2004), but the ability to use spectroscopic redshifts for lenses is a major advantage to doing lensing with the SDSS. The high statistical power has been accompanied by a more careful investigation of systematic errors, such as calibration biases and intrinsic alignments, which for the SDSS are currently around 10 per cent and therefore already dominate the error budget (Mandelbaum et al. 2005a, hereafter M05).

In this work, we seek to use g–g weak lensing to explore the galaxy–DM connection for particular subsamples of lenses. By comparison with the predicted signal from a halo model, as done for simulations in Mandelbaum et al. (2005b), we can extract average central halo masses and satellite fractions. These calculations are done as a function of morphology and of environment, in samples selected based on both stellar masses and luminosity. We expect that the divisions by morphology and by environment may be related, due to the relationships between colour and environment, with red galaxies typically found in overdense regions (Davis & Geller 1976; Dressler 1980; Postman & Geller 1984; Balogh et al. 1998, 1999; Carlberg et al. 2001; Blanton et al. 2003a; Hogg et al. 2003; Balogh et al. 2004a,b; Hogg et al. 2004; Croton et al. 2005). By determining average central halo masses and satellite fractions as a function of these parameters, we hope to gain some insight into processes of galaxy formation, and ultimately into the galaxy–DM connection. We note that this approach has been used before, by Guzik & Seljak (2002) based on data in McKay et al. (2001), but with a simpler form of the halo model, with a much smaller sample of lenses so lower statistical power, and only using the luminosities, not stellar masses. Due to our larger sample of lenses, our better-understood calibration and our inclusions of stellar masses which are better tracers of stellar and DM content than luminosities, this work constitutes a significant improvement over that one. Another recent work, Hoekstra et al. (2005), used stellar masses for RCS data derived from $B - V$ colours from Canada–France–Hawaii Telescope photometry in order to derive halo masses as a function of luminosity, and star formation efficiencies as a function of morphology, but used only isolated lenses and thus did not derive satellite fractions. Furthermore, the lack of spectroscopic redshifts for lenses in that work, which allow the derivation of stellar masses via spectral indicators and the computation of the lensing signal

as a function of transverse separation in this work, complicates the analysis. Halo model analysis of g–g autocorrelations has been done observationally by several groups (van den Bosch, Yang & Mo 2003; Cooray 2005; Zehavi et al. 2005), and this halo model analysis of galaxy–DM cross-correlations is, in many ways, complementary to that approach.

We begin by introducing the g–g lensing formalism and the halo model that is used to extract information about central halo masses and satellite fractions in Section 2. Section 3 includes a description of the SDSS data used for this analysis. We present the lensing signal and the halo model fits in Section 4, and interpretation of these results. We conclude in Section 5 with a summary of our findings.

Here, we note the cosmological model and units used in this paper. All computations assume a flat Λ cold dark matter universe with $\Omega_m = 0.3$, $\Omega_\Lambda = 0.7$ and $\sigma_8 = 0.9$. Distances quoted for transverse lens–source separation are comoving (rather than physical) h^{-1} kpc, where $H_0 = 100\,h\,\mathrm{km\,s^{-1}\,Mpc^{-1}}$. Likewise, $\Delta\Sigma$ is computed using the expression for Σ_c^{-1} in comoving coordinates, equation (4). In the units used, H_0 scales out of everything, so our results are independent of this quantity. All confidence intervals in the text and tables are 95 per cent confidence level (CL) (2σ) unless explicitly noted otherwise.

2 WEAK LENSING FORMALISM AND HALO MODEL

Galaxy–galaxy weak lensing provides a simple way to probe the connection between galaxies and matter via their cross-correlation function

$$\xi_{g,m}(\boldsymbol{r}) = \left\langle \delta_g(\boldsymbol{x})\delta_m^*(\boldsymbol{x} + \boldsymbol{r}) \right\rangle, \tag{1}$$

where δ_g and δ_m are overdensities of galaxies and matter, respectively. This cross-correlation can be related to the projected surface density

$$\Sigma(R) = \overline{\rho} \int [1 + \xi_{g,m}(\sqrt{R^2 + \chi^2})]\,\mathrm{d}\chi \tag{2}$$

(where $r^2 = R^2 + \chi^2$), which is then related to the observable quantity for lensing,

$$\Delta\Sigma(R) = \gamma_t(R)\Sigma_c = \overline{\Sigma}(<R) - \Sigma(R), \tag{3}$$

where the second relation is true only for a matter distribution that is axisymmetric along the line of sight. This observable quantity can be expressed as the product of two factors, a tangential shear γ_t and a geometric factor

$$\Sigma_c = \frac{c^2}{4\pi G} \frac{D_S}{D_L D_{LS}(1 + z_L)^2}, \tag{4}$$

where D_L and D_S are angular diameter distances to the lens and source, D_{LS} is the angular diameter distance between the lens and source, and the factor of $(1 + z_L)^{-2}$ arises due to our use of comoving coordinates. For a given lens redshift, Σ_c^{-1} rises from zero at $z_S = z_L$ to an asymptotic value at $z_S \gg z_L$; that asymptotic value is an increasing function of lens redshift.

There are two basic approaches that can be used to extract information about properties of the galaxy distribution (e.g. halo masses and satellite fractions) from the g–g lensing signal. The first approach is to compare directly against N-body simulations (Guzik & Seljak 2001; Yang et al. 2003; Tasitsiomi et al. 2004; Weinberg et al. 2004). While this approach has the advantage of being fairly direct, it has the disadvantage that even assuming a given cosmological model, the process of galaxy formation is not sufficiently

understood to result in unique predictions for that model. When combined with the fact that the cosmological model is not itself fully determined yet, one would have to expend tremendous computational resources to run multiple simulations with different cosmologies and models. Furthermore, current simulations still suffer from a limited dynamical range, in the sense that they require a high mass and force resolution to resolve individual galaxies and their associated DM haloes, while at the same time they must also have sufficiently large volume to simulate a representative region of the universe. Several simulations of varying box size are thus needed to cover the whole observational range in luminosity and scale.

Another approach to model the relation between galaxies and DM is to use a halo model (e.g. Peacock & Smith 2000; Seljak 2000; Scoccimarro et al. 2001; Cooray & Sheth 2002), which in this application can be used as a phenomenological description of the processes that determine the lensing signal for particular types of galaxies. Comparison of the halo model predicted signal versus the real signal can lead to the determination of quantities such as the virial mass distribution and the fraction of these galaxies that are satellites, which are useful quantities for constraining the galaxy formation models and cosmological models. This approach has the advantage that it is not as computationally expensive, so large areas of parameter space can be explored very quickly, but must be compared against simulations to ensure that it works properly. Mandelbaum et al. (2005b) compared the halo model with simulations, and determined that central halo masses (M_{cent}) and satellite fractions (α) can be extracted adequately from the lensing signal, provided that the distribution of central halo masses is not too broad (σ_M/M_{cent} less than about a factor of 2), or that corrections be applied if it is broad. Thus, in this paper we use those results to extract information from the measured weak lensing signal from the SDSS using halo model fits, as has already been done by Seljak et al. (2005) (including variation of the results with Ω_{m} and σ_8, for which we refer the reader to that paper). The halo model used here is the same as that from Mandelbaum et al. (2005b), to which the interested reader can refer for details. Here, we give only the basic details necessary to understand this paper.

The halo model can be used to derive the galaxy–DM cross-power spectrum $P_{\text{g,DM}}(k)$ by considering separately the contributions of central galaxies (which lie in haloes that are not contained within another halo) and satellite galaxies (which lie in subhaloes contained entirely within another halo). There are then one-halo or Poisson terms, derived from the cross-correlation of the galaxy with its own matter distribution (for central galaxies and satellites) and with that of the host halo (for satellites), and a halo–halo (h–h) term derived from the cross-correlation with the mass of other haloes. The latter is negligible on the small ($<2\,h^{-1}$ Mpc) scales to which we limit ourselves in this work. Therefore, rather than attempting to fit for it by fitting to the bias, we fix the bias by doing the halo model fits without the h–h term to get the halo mass, then using $b(M)$ from Seljak & Warren (2004) to redo the fits for M_{cent} and α with the appropriate value of bias fixing the h–h term. Including this correction makes very little difference on the final results, as expected since on small scales the h–h term is negligible. For the same reason we ignore the morphology dependence of halo bias, suggested by recent simulations Gao, Springel & White (2005) that studied the dependence of clustering on halo formation time. For splits by local density, we use the appropriate $b(M)$ for that mass for the high-density samples (again, ignoring dependence of bias on local environment), and do not include a h–h term at all for low-density samples.

The one-halo term requires various ingredients, such as the halo mass function dn/dM, the radial profile of DM within haloes $\rho(r)$, the radial distribution of galaxies within groups and clusters, the conditional halo mass probability distribution, and the tidal stripping of satellites in clusters. The DM profiles are assumed here to be NFW profiles (Navarro, Frenk & White 1996) with concentration parameter (Bullock et al. 2001; Eke, Navarro & Steinmetz 2001)

$$c_{\text{DM}} = 10 \left[\frac{M_{\text{cent}}}{M_{\text{nl}}(z)} \right]^{-0.13}, \tag{5}$$

where $M_{\text{nl}}(z)$, the non-linear mass scale, is defined such that the rms linear density fluctuation extrapolated to redshift z within a sphere containing mass M_{nl} is equal to $\delta_{\text{c}} = 1.686$, the linear overdensity at which a spherical perturbation collapses. $M_{\text{nl}}(z)$ is a cosmology-dependent parameter. The satellites are assumed to be distributed according to an NFW profile with concentration parameter $c_{\text{g}} = c_{\text{DM}}$ (Carlberg, Yee & Ellingson 1997; Peacock & Smith 2000; Gao et al. 2004a), though the importance of this assumption – which may overestimate c_{g} (Carlberg et al. 1997; Lin, Mohr & Stanford 2004; Hansen et al. 2005; Nagai & Kravtsov 2005) – will be explored later. Unfortunately, since c_{g} is, in general, poorly determined from previous data and our own, we cannot fit for it and must assume some model.

The conditional halo mass probability distribution for a given lens luminosity L_i is modelled as having two parts, p^{C} (central) and p^{NC} (non-central), using a free parameter α, the satellite fraction

$$p(M; L_i) = (1 - \alpha)p^{\text{C}}(M; L_i) + \alpha p^{\text{NC}}(M; L_i). \tag{6}$$

For haloes hosting a central galaxy, we model the luminosity–halo mass relationship as a delta-function; for haloes hosting non-central galaxies, we assume that there is a relationship between the number of galaxies of this luminosity and the host halo mass, $\langle N \rangle(M; L) \propto M^\epsilon$ (the host halo number; Kauffmann et al. 1999; Kravtsov et al. 2004; Lin et al. 2004; Zehavi et al. 2005). As in Mandelbaum et al. (2005b), we use $\langle N(M) \rangle \propto M^\epsilon$ with $\epsilon = 1$ for $M > 3M_{\text{cent}}$ and $\epsilon = 2$ below that value. This result was shown there to match the simulations from Tasitsiomi et al. (2004) quite well, and the power-law exponent $\epsilon = 1$ above a cut-off is consistent with semi-analytic models of galaxy formation (Kauffmann et al. 1999; Guzik & Seljak 2002), N-body simulations (Kravtsov et al. 2004; Zehavi et al. 2005), and observational measurements (Jing, Mo & Boerner 1998; Lin et al. 2004; Cooray 2006; Zehavi et al. 2005). Since some of the observational analyses (e.g. Zehavi et al. 2005) suggest that significantly different values of ϵ may still be allowed, we explore in this paper the dependence of our results on its assumed value.

Finally, our model for tidal stripping is that satellites have half of their mass stripped, which corresponds to truncating the central density profile at $0.4r_{\text{vir}}$ (beyond which we use $\Delta\Sigma \propto R^{-2}$ as for a point mass). This assumption is consistent with the average mass loss for subhaloes observed in cosmological simulations (Gao et al. 2004b; Nagai & Kravtsov 2005). We will attempt to say something about this assumption by looking at galaxies in low- and high-density regions separately.

After using these inputs to obtain the galaxy–DM cross-power spectrum $P_{\text{g,DM}}(k)$, we can Fourier transform to obtain the correlation function $\xi_{\text{g,DM}}(R)$, integrate once to get $\Sigma(R)$ via equation (2), and integrate again to obtain $\Delta\Sigma(R)$ via equation (3).

Using the precomputed signal, we compare against the observed lensing signal to derive two properties of the lens sample: the halo mass M_{cent} of the central galaxy, defined in terms of the radius such that the overdensity within is equal to 180 times the mean density

(roughly 30 per cent larger than the mass M_{200} defined within the radius where the overdensity is equal to 200 times critical density, another definition of virial radius and mass that is often used); and the fraction of galaxies in the sample that are satellites residing in a larger halo (i.e. a group or cluster), α. Note that we do not attempt to measure any other parameters of the central halo mass distribution besides the central halo mass. In these fits, the average redshift of the sample is relatively unimportant compared to the cosmology (Ω_m and σ_8), for which variation of the best-fitting satellite fraction may be significant (Seljak et al. 2005).

One issue raised in Mandelbaum et al. (2005b) is the question of the meaning of the best-fitting halo mass; for samples of lenses with broad central halo mass distributions, such that the mean and median are significantly different, the best-fitting masses must be adjusted upwards if one is interested in the mean (as we are), and downwards if one is interested in the median. We attempt to isolate samples of lenses with narrow distributions in central halo mass in two ways: first, by using bins narrow in luminosity (half or one absolute magnitude or a factor of 1.6–2.5 in luminosity) or stellar mass (a factor of 2 wide) and secondly, by splitting the sample within those bins based on morphology into early- versus late-types. Consequently, we use the small corrections to the best-fitting masses determined from table 1 in Mandelbaum et al. (2005b) for the case of no scatter in the $M(L)$ relationship. Details of these corrections will be given in Section 4.2.

3 DATA

The data used here are obtained from the SDSS (York et al. 2000), an ongoing survey to image roughly π steradians of the sky, and follow up approximately one million of the detected objects spectroscopically (Eisenstein et al. 2001; Richards et al. 2002; Strauss et al. 2002). The imaging is carried out by drift-scanning the sky in photometric conditions (Hogg et al. 2001; Ivezić et al. 2004), in five bands (*ugriz*) (Fukugita et al. 1996; Smith et al. 2002) using a specially designed wide-field camera (Gunn et al. 1998). These imaging data are the source of the large-scale structure (LSS) sample that we use in this paper. In addition, objects are targeted for spectroscopy using these data (Blanton et al. 2003b) and are observed with a 640-fibre spectrograph on the same telescope (Gunn et al. 2006). All of these data are processed by completely automated pipelines that detect and measure photometric properties of objects, and astrometrically calibrate the data (Lupton et al. 2001; Pier et al. 2003; Tucker et al. 2005). The SDSS is well underway, and has had five major data releases (DRs) (Stoughton et al. 2002; Abazajian et al. 2003, 2004; Finkbeiner et al. 2004; Abazajian et al. 2005; Adelman-McCarthy et al. 2006).

3.1 Lenses

The galaxies used as lenses are those targeted as the DR4 Main spectroscopic sample (4783 deg^2), with calibration as described in Finkbeiner et al. (2004). Here we describe the quantities used for classifying the lenses into subsamples: morphology, stellar masses, luminosities and density. We note that all samples described here are flux-limited, not volume-limited, with the flux limit nominally $r < 17.77$ (Petrosian, extinction-corrected) but actually varying slightly in a known way across the survey area. Only those lens galaxies with redshifts $0.02 < z < 0.35$ were used.

An important feature of this work is the splitting of lens samples based on morphology within each stellar mass or luminosity subsample, since predictions of the quantities we are measuring may differ significantly for spiral and elliptical galaxies. This split

is carried out in practice by requiring that the parameter frac_deV output from the PHOTO pipeline be $\geqslant 0.5$ for early-types, <0.5 for late-types. This parameter is determined by fitting the galaxy profile to frac_deV times the best-fitting de Vaucouleurs profile plus $(1 - \text{frac\_deV})$ times the best-fitting exponential profile (and requiring $0 \leqslant \text{frac\_deV} \leqslant 1$) in each band separately. For this work, to reduce the noise, we use the unweighted average over the *g*, *r* and *i* bands. In practice, frac_deV is highly correlated with galaxy colours. Strateva et al. (2001) studied the effectiveness of morphological classification using either colours or de Vaucouleurs and exponential profile likelihoods for a sample of spectroscopic galaxies for which morphological classification was determined using spectral indices. The result is that for early-types, selection by *r*-band frac_deV results in 96 per cent completeness, and is 76 per cent reliable (that is, 96 per cent of the early-types were indeed classified as early-types, and 76 per cent of those classified as early-types were actually early-types). For late types, the completeness was 55 per cent, and the classification was 90 per cent reliable. However, since we use the average of the results in *g*, *r* and *i*, rather than just the results in *r*, and a more recent version of PHOTO, it is likely that the results of classification using frac_deV for this paper are even better than those quoted there. We note that selection by $u - r$ colour yielded 98 per cent completeness and 83 per cent reliability for early-types, and 72 per cent completeness and 96 per cent reliability for late-types, a slight improvement in the results over classification using profiles in that work, though our use of profile information from three bands and a more recent version of PHOTO may decrease that advantage.

Stellar mass estimates were obtained from the spectra using the same techniques as in Kauffmann et al. (2003), but for the full DR4 sample. A library of 32 000 model star formation histories generated using the Bruzual & Charlot (2003) population synthesis models and the measured $D_n(4000)$ and $H\delta_A$ indices (Tremonti et al. 2004) are used to obtain a median likelihood estimate of the *z*-band mass-to-light ratio (M/L) for each galaxy. By comparing the colour predicted by the best-fitting model to the observed colour of the galaxy, the attenuation of the starlight due to dust is also estimated. The corrected *z*-band magnitude and the M/L_z together yield an estimate of the stellar mass. These estimates have 95 per cent confidence ranges of around ±40 per cent. Comparison of these measures of stellar mass, which are better measures of the mass in stars than luminosity, against the best-fitting halo masses will allow us to learn about the efficiency of conversion of baryons in the halo to stars. We define this efficiency via the relation

$$\eta = \frac{M_{\text{stellar}}}{M_{\text{cent}}} \frac{\Omega_m}{\Omega_b} = \frac{M_{\text{stellar}}}{M_{\text{cent}} f_b} \tag{7}$$

where f_b is the cosmological baryon fraction. We note that this quantity is not the same as the traditional definition of star formation efficiency, the rate at which stars are forming compared to the available mass or surface mass density in H I or molecular gas. Hence, we use the term conversion efficiency rather than star formation efficiency when describing these results. There are two differences between these quantities. First, the star formation efficiency denotes the fraction of those baryons that have cooled off and formed part of the galaxy that then were included in stars. On the other hand, as shown in equation (7), the conversion efficiency assumes that the baryon fraction in the galaxy is equal to the cosmological one, thus ignoring the fact that some significant fraction of baryons actually are not in galaxies, but are located in, e.g. the hot gas in clusters or warm–hot gas on the outskirts of galaxies. Furthermore, equation (7) includes all baryonic matter, such as helium, whereas

Table 1. The stellar mass subsamples used in this analysis, including mean weighted redshifts within each bin, the total number of galaxies and the fraction of spirals.

Sample	$M_{stellar}$ $(10^{10}\,M_{\odot})$	N_{gal}	$\langle z \rangle$	$\langle M_{stellar} \rangle$ $(10^{10}\,M_{\odot})$	f_{spiral}
sm1	[0.5, 1.0]	23 474	0.060	0.74	0.74
sm2	[1.0, 2.0]	40 952	0.070	1.5	0.60
sm3	[2.0, 4.0]	66 503	0.085	2.9	0.46
sm4	[4.0, 8.0]	90 019	0.11	5.7	0.32
sm5	[8.0, 16.0]	82 734	0.13	11.0	0.20
sm6	[16.0, 32.0]	39 729	0.16	21.0	0.11
sm7	[32.0, 64.0]	8 096	0.19	40.0	0.05

Table 2. The luminosity subsamples used in this analysis, including mean weighted redshifts and luminosities within each bin, the total number of galaxies and the fraction of spirals.

Sample	M_r	N_{gal}	$\langle z \rangle$	$\langle L/L_* \rangle$	f_{spiral}
L1	$-17 \geqslant M_r > -18$	10 047	0.032	0.075	0.80
L2	$-18 \geqslant M_r > -19$	29 730	0.047	0.19	0.69
L3	$-19 \geqslant M_r > -20$	85 766	0.071	0.46	0.53
L4	$-20 \geqslant M_r > -21$	141 976	0.10	1.1	0.35
L5f	$-21 \geqslant M_r > -21.5$	60 994	0.14	2.1	0.23
L5b	$-21.5 \geqslant M_r > -22$	34 920	0.17	3.2	0.16
L6f	$-22 \geqslant M_r > -22.5$	13 067	0.20	4.9	0.08
L6b	$-22.5 \geqslant M_r > -23$	2 933	0.22	7.7	0.05

the star formation efficiency is defined relative to mass of hydrogen only. Because of these differences in definitions, our results for baryon conversion efficiency are also lower limits on the star formation efficiency.

Table 1 gives information about the stellar mass bins used for this work, each of which is a factor of 2 wide: the numbers of galaxies in each bin, the mean redshift within each bin (determined using the weights from the lensing analysis), and the fraction of galaxies classified as spirals (f_{spiral}). We note that because of the statistical error on each estimate, the bins are actually equivalent to top-hats of a factor of 2 wide in stellar mass convolved with approximate Gaussians with $\sigma/\langle M_{stellar} \rangle \sim 0.2$. Throughout this work, stellar masses $M_{stellar}$ are given in units of $M_{\odot}$, having been computed with $h = 0.7$ as in Kauffmann et al. (2003).

We also must consider systematic uncertainties in our results due to assumptions that are involved in the stellar mass determination. A full discussion can be found in Kauffmann et al. (2003); the main uncertainty that will affect our results is the uncertainty due to the initial mass function (IMF), since we must assume that the locally observed IMF applies universally. Changing from the IMF given by Kroupa (2001) to another IMF (assuming that it is uniform across all samples), such as the Salpeter IMF, may rescale all the stellar mass values, and therefore the derived conversion efficiencies, by a fixed value of up to 30 per cent. However, we note that Cappellari et al. (2006) found with a sample of $>L_*$ ellipticals that the measured M/L values appear inconsistent with the Salpeter IMF, which predicts too much mass, so this value of 30 per cent is likely conservative. To address the question of whether the IMF really is uniform across all samples, we note that Kroupa (2001) found no evidence for significant variations in the IMF within our own galaxy; assuming that the results of Cappellari et al. (2006) represent typical elliptical galaxies, and the Milky Way is a typical spiral, we can then infer that the IMF of spirals and ellipticals is not significantly different. Thus, even if the global IMF leads to some overall rescaling of the stellar mass values, many of the results which we will present are in the form of trends of conversion efficiency with stellar mass, or comparisons between two different lens samples at fixed stellar mass, which are still valid regardless of this systematic uncertainty.

Luminosities were determined using the r-band Petrosian apparent magnitudes (extinction-corrected using the reddening maps from Schlegel, Finkbeiner & Davis 1998), k-corrections to $z = 0.1$ (the sample median) from KCORRECT v1_11 (Blanton et al. 2003c), passive luminosity evolution correction from Blanton et al. (2003b), and the distance modulus determined using $h = 1$, yielding $M_r = m + 1.6(z - 0.1) - (K + DM)$. These luminosities may be underestimated at typically the 10–20 per cent level (West et al.

in preparation) due to the sky-subtraction systematic (Adelman-McCarthy et al. 2006; M05), an overestimate in the local sky estimate within $\sim$90 arcsec of bright ($r < 18$) galaxies and stars, thus affecting the entire lens sample at some level. The actual underestimation varies with apparent magnitude and size, and changes the estimated M/L; since the effect has not been well quantified for the full sample and is within the 95 per cent CL, we have applied no correction.

One possible systematic in the comparisons between stellar mass and luminosity is the fact that the luminosity is the full Petrosian magnitude (which contains essentially all the light of an exponential profile, and about 80 per cent of the light in a de Vaucouleurs profile), whereas the stellar mass is estimated using spectra measured using a 3-arcsec aperture. Kauffmann et al. (2003) discuss this 'aperture bias' in detail, and while it is found to influence the results at some level, the variation in $M_{stellar}/L$ due to this systematic are insignificant compared to its variation with galaxy properties such as luminosity and profile type (parametrized there using the concentration index).

In order to obtain M/L, solar luminosities were determined using results from Blanton et al. (2003b) with $M_* = -20.44$ and $M_{solar} = 4.76$, yielding luminosities in $h^{-2}\,L_{\odot}$ ($L_* = 1.2\,h^{-2} \times 10^{10}\,L_{\odot}$). Relevant information for luminosity subsamples is shown in Table 2, including numbers of galaxies, mean weighted redshifts and luminosities, and spiral fractions. We note that we split the two brightest bins into half-magnitude bins, because we would like the opportunity to better constrain the variation of mass with light in that regime, and because the central halo mass distribution may become wider at higher luminosities since some of the galaxies are brightest cluster galaxies (BCGs) of clusters with large halo masses, and others are field galaxies hosted by smaller haloes, giving a broader halo mass distribution at the high-luminosity end.

Finally, we need a measure of the local galaxy environment. Many estimators, including nth nearest neighbour (3D or in projection), counts in an aperture (again, 3D or in projection), and Voronoi volumes, have been used in the literature (for example, Ramella et al. 2001; Marinoni et al. 2002; Hogg et al. 2003; Balogh et al. 2004b; Blanton et al. 2005b; Cooper et al. 2005). Here, we choose a very simple one, spectroscopic galaxy counts in cylinders of radius $1\,h^{-1}$ Mpc and line-of-sight length $\Delta v = \pm1200\,km\,s^{-1}$. These numbers are compared to the number of random points in the same cylinders, thus taking into account the angular and radial variations in number density, survey boundaries, and other issues. While galaxies excluded in the spectroscopic survey because of fibre collisions are not used for the stellar mass study (since they lack spectra), they are used for the density estimates in order to avoid underestimating the environment measure in rich clusters. The galaxies without

spectra due to fibre collisions are given redshifts equal to those of the nearest neighbour. We note that because the environment measurement requires a careful knowledge of the survey completeness as a function of position, only those galaxies included in the area covered by the LSS DR4 sample from the NYU Value-Added Galaxy Catalogue (Blanton et al. 2005a) were used to obtain environment estimates.

Our estimates were derived using 20 times as many random points as real galaxies; we note that for higher redshifts, these environment estimates can be quite noisy or may fail entirely, because the radial selection function leads to a low density of objects. Furthermore, galaxies at the lower-redshift limit or near survey boundaries may not have environment estimates if no random galaxies were found in the cylinders around them; thus, when splitting the sample at the median density within each stellar mass or luminosity bin, only some fraction of the sample was used (ranging from 93 per cent for bins at $L < \sim L_*$, down to 40 per cent for the brightest galaxies). Fortunately, the lensing signal itself provides a reasonable test of the environment estimate, because we can see whether the signal at 1–$2\,h^{-1}$ Mpc scales is consistent with the lens sample primarily being in the field or in groups and clusters. At fixed luminosity or stellar mass, the spiral sample (defined by frac_deV < 0.5) had a lower median and mean environment estimate than ellipticals, as expected from previous studies cited in Section 1.

Because of the need for spectra to determine stellar masses, our sample must exclude galaxies for which spectra were not obtained due to fibre collisions. Fibres cannot be placed closer than 55 arcsec ($\sim 80\,h^{-1}$ kpc at $z \sim 0.1$), so if two targets are closer than this separation, only one will have a spectrum. This restriction is alleviated in roughly one-third of the sky by the use of overlapping plates, but none the less, roughly 7 per cent of targets do not have spectra. This loss of targets is naturally worse in high-density regions, and will therefore tend to affect the satellite contribution, decreasing it in a scale-dependent way, and therefore changing its shape. However, as our results will show, we are not highly sensitive to the shape of the satellite contribution.

3.2 Sources

The source sample is the same as that from M05, who obtained shapes for more than 30 million galaxies in the SDSS imaging data down to magnitude $r = 21.8$ (i.e. four magnitudes fainter than the SDSS spectroscopic limit). This section briefly describes the M05 pipeline, also known as Reglens.

The M05 pipeline obtains galaxy images in the r and i filters from the SDSS 'atlas images' (Stoughton et al. 2002). The basic principle of shear measurement using these images is to fit a Gaussian profile with elliptical isophotes to the image, and define the components of the ellipticity

$$(e_+, e_\times) = \frac{1 - (b/a)^2}{1 + (b/a)^2}(\cos 2\phi, \sin 2\phi), \tag{8}$$

where b/a is the axis ratio and ϕ is the position angle of the major axis. This is then an estimator for the shear,

$$(\gamma_+, \gamma_\times) = \frac{1}{2\mathcal{R}}\langle(e_+, e_\times)\rangle, \tag{9}$$

where $\mathcal{R} \approx 0.87$ is called the 'shear responsivity' and represents the response of the ellipticity (equation 8) to a small shear (Kaiser, Squires & Broadhurst 1995; Bernstein & Jarvis 2002). In practice, a number of corrections need to be applied to obtain the ellipticity. The most important of these is the correction for the smearing and circularization of the galactic images by the point spread function

(PSF); M05 uses the PSF maps obtained from stellar images by the PSP pipeline (Lupton et al. 2001), and corrects for these using the re-Gaussianization technique of Hirata & Seljak (2003). Re-Gaussianization corrects for the PSF while taking into account the non-Gaussianity both of the PSF and of the galaxy profile. A smaller correction is for the optical distortions in the telescope: ideally the mapping from the sky to the CCD is shape-preserving (conformal), but in reality this is not the case, resulting in a non-zero 'camera shear'. In the SDSS, this is a small effect (of the order of 0.1 per cent) which can be identified and removed using the astrometric solution (Pier et al. 2003). Finally, a variety of systematics tests are necessary to determine that the shear responsivity $\mathcal{R}$ has in fact been determined correctly. We refer the interested reader to M05 for the details of these corrections and tests.

M05 includes a lengthy discussion of shear calibration biases in this catalogue; we will only summarize these issues briefly here. Our source sample is divided into three subsamples: $r < 21, r > 21$ and high-redshift luminous red galaxies (LRGs; Eisenstein et al. 2001), defined using colour and magnitude cuts as in M05 using selection criteria related to those from Eisenstein et al. (2001) and Padmanabhan et al. (2005). Using simulations from Hirata & Seljak (2003) to estimate the PSF dilution correction and analytical models for selection biases and other issues that affect shear calibration, we place 2σ limits on the multiplicative shear calibration bias of $[-5, 12]$ per cent for $r < 21$, $[-8, 18]$ per cent for $r > 21$, and $[-6, 19]$ per cent for LRGs.

As shown in equation (3), the lensing signal $\Delta\Sigma$ is a product of the shear and factors involving lens and source redshifts. Since the lenses have spectroscopic redshifts, the primary difficulty is determining the source redshift distribution. We take three approaches, all described in detail in M05. For the $r < 21$ sources, we use photometric redshifts and their error distributions determined using a sample of galaxies in the Groth strip with redshifts from DEEP2 (Davis et al. 2003; Madgwick et al. 2003; Coil et al. 2004; Davis, Gerke & Newman 2004), and require $z_S > z_L + 0.1$ to avoid contamination from physically associated lens–source pairs. For the $r > 21$ sources, we use redshift distributions from DEEP2. For the high-redshift LRGs, we use photometric redshifts and their error distributions determined using data from the two-degree Field (2dF)-Sloan LRG and Quasar Survey (2SLAQ) and presented in Padmanabhan et al. (2005).

Finally, we have placed constraints on other issues affecting the calibration of the lensing signal, such as the sky-subtraction problem, intrinsic alignments, magnification bias, star–galaxy separation and seeing-dependent systematics. As shown in M05 the calibration of the signal using the three source samples agrees to within 10 per cent, with a total 1σ calibration uncertainty estimated at 7 per cent ($r < 21$) or 10 per cent ($r > 21$ and LRG).

3.3 Signal computation

Here we describe the computation of the lensing signal. Lens–source pairs are assigned weights according to the error on the shape measurement via

$$w_{LS} = \frac{\Sigma_c^{-2}}{\sigma_S^2 + \sigma_{SN}^2}, \tag{10}$$

where σ_{SN}^2, the intrinsic shape noise, was determined as a function of magnitude in fig. 3 of M05. The factor of Σ_c^{-2} downweights pairs that are close in redshift.

Once we have computed these weights, we compute the lensing signal in 46 logarithmic radial bins from $20\,h^{-1}$ kpc to $2\,h^{-1}$ Mpc as

a summation over lens–source pairs via

$$\Delta\Sigma(R) = \frac{\sum_{LS} w_{LS} \gamma_t^{(LS)} \Sigma_c}{2\mathcal{R} \sum_{LS} w_{LS}},$$ (11)

where the factor of 2 arises due to our definition of ellipticity.

There are several additional procedures that must be done when computing the signal (for more detail, see M05). First, the signal computed around random points must be subtracted from the signal around real lenses to eliminate contributions from systematic shear. Secondly, the signal must be boosted, i.e. multiplied by $B(r) = n(r)/n_{rand}(r)$, the ratio of the number density of sources relative to the number around random points, in order to account for dilution by sources that are physically associated with lenses, and therefore not lensed.

In order to determine errors on the lensing signal, we divide the survey area into 200 bootstrap subregions, and generate 2500 bootstrap-resampled data sets. To determine errors on fit parameters, we perform the fits on each bootstrap-resampled data set, and use the distribution in parameter space to determine confidence intervals.

4 RESULTS

4.1 Lensing signal

In Fig. 1, we show the lensing signal in stellar mass bins with 1σ errors, for spiral (frac_deV < 0.5) and elliptical (frac_deV $\geqslant$ 0.5) galaxies, with the best-fitting halo model signal (with parameters to be described in Section 4.2). Fig. 2 shows the same for luminosity

bins; the signal was noisy enough for the brightest bin (L6b) that errors could not be determined on fits, so that bin is not shown. Finally, Fig. 3 shows the results in luminosity bins for low- and high-density samples of ellipticals only. The results have been rebinned for easier viewing; correlations between radial bins are minimal at small radius, and reach a maximum of about 0.2–0.3 at the outermost bins for the lower luminosity or stellar mass bins (at lower z) and are negligible at all radii for the brighter bins. While the model fits are shown on the plots, we defer discussion of the best-fitting parameters to the following sections, and focus here on a comparison of the lensing signal.

First, we consider Fig. 1. There appears to be some detection of signal on all scales for all but the lowest bin, $5 \times 10^9 < M_{stellar}/M_\odot < 10^{10}$. For sm2–sm4, comprising $(1–8) \times 10^{10}\,M_\odot$, the signal for early- and late-types appears statistically consistent for $r < {\sim}100\,h^{-1}$ kpc, indicating that the average halo masses (and therefore conversion efficiencies) for the two types of galaxies are similar. For sm5 and sm6, comprising $(8–32) \times 10^{10}\,M_\odot$, the signal on small scales is larger for early-types than for late-types, indicating a larger average halo mass for early-types, so stellar mass is no longer a good tracer of halo mass for this range of stellar masses. This result is not entirely surprising, since for these bins, some fraction of the red galaxies are LRGs that may be the BCGs of clusters, so the halo masses determined using lensing are actually the masses of the entire cluster rather than of individual galaxies. On larger scales, the signal for early-types is higher than for late-types for each stellar mass bin to a degree that is highly statistically significant, consistent with previous findings that red galaxies reside in denser environments than blue galaxies.
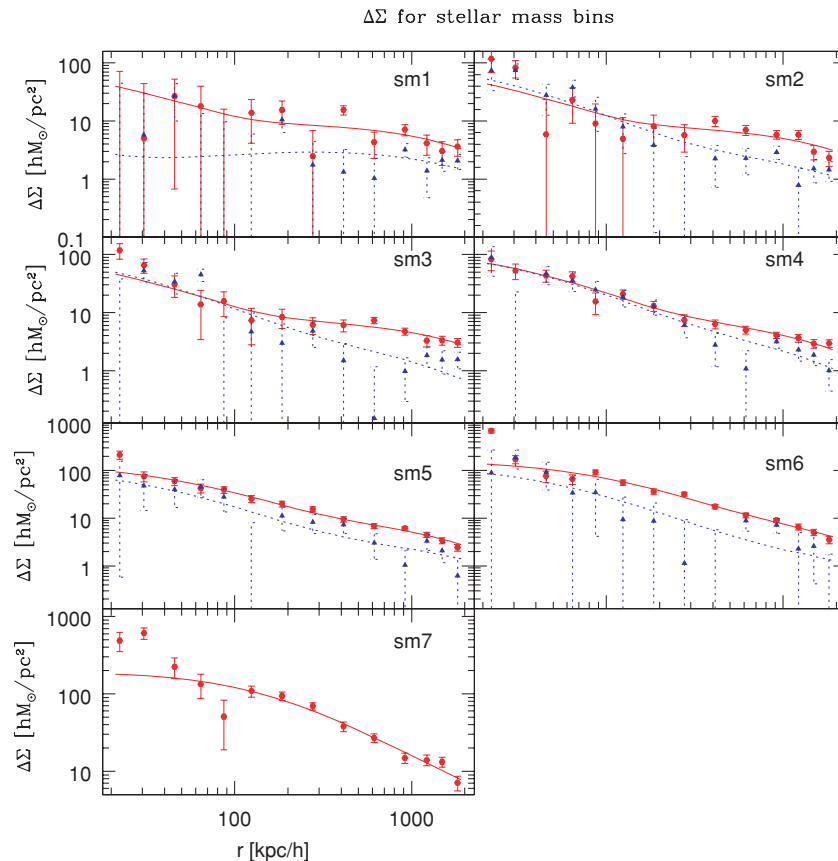

Figure 1. $\Delta\Sigma$ in stellar mass bins for early (red hexagons, solid line) and late-type (blue triangles, dashed line) galaxies. For the highest stellar mass bin, only the signal for early-types is shown since they are 95 per cent of the sample. All errors are 1σ.
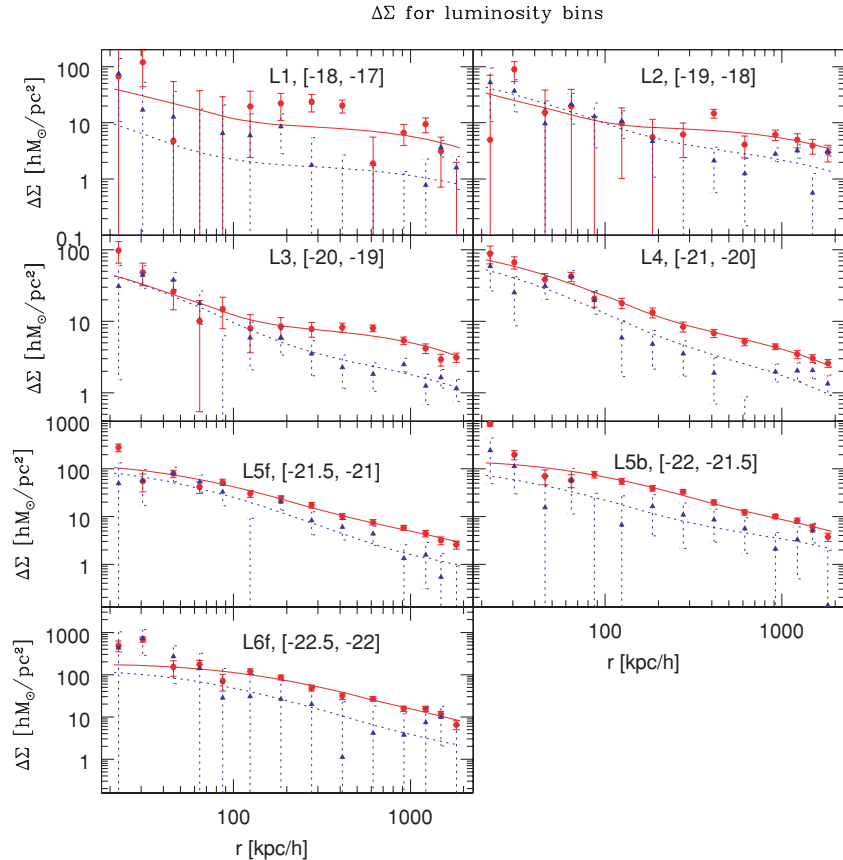
ΔΣ for luminosity bins

Figure 2. $\Delta\Sigma$ with best-fitting halo model in luminosity bins for early (red hexagons, solid line) and late-type (blue triangles, dashed line) galaxies. All errors are 1σ.

Next, we consider Fig. 2. The detection is marginal in L1 and L2, comprising magnitudes $-19 \leqslant M_r < -17$. For the bins with a robust detection, L3 (with $\langle L/L_* \rangle = 0.46$) is the only one for which the signal for early and late-types appears to be highly consistent at small scales; at higher luminosity, it appears to be higher for early-types. On large scales, the signal for early-types is again larger than for late-types for all luminosity bins, indicating a tendency for early-types to be in denser environments.

Finally, we consider Fig. 3, which shows $\Delta\Sigma$ in luminosity bins for early-type galaxies only, with the sample divided at the median environment measure in that bin. We remind the reader that environment estimates were not obtained for a large fraction of the galaxies in the brightest bins due to the limitations of the environment estimator, so few lenses were used for those bins. For L1–L5, it is apparent from the signal on $r > 300\,h^{-1}$ kpc that the environment split efficiently separates the galaxies into those that reside in overdense versus underdense regions. This separation is particularly marked for L3 and L4, with the signal on $1–2\,h^{-1}$ Mpc scales differing between the high- and low-density samples by more than an order of magnitude. For the brightest bins, the difference is less striking; it is possible that our environment estimator is simply too noisy at higher redshifts, or that enough of the L6 early-type galaxies reside in groups and clusters that the environment simply does not vary much across the bin, leading to a small variation in signal. For all bins, the signal on small scales does not vary significantly with the environment. As we show below, the L_* high-density sample is dominated by satellites. We see that the tidal stripping of DM around satellites inside groups and clusters cannot be maximally efficient,

since this would have been seen as a suppression of signal on small scales.

4.2 Halo model fits

Here, we discuss the goodness-of-fit for the halo model fits before proceeding to discussions of the best-fitting parameters. However, we note that the values of χ^2 are not expected to follow the usual χ^2 distribution because of the noisiness of bootstrap covariance matrices (see Hirata et al. 2004 for a fuller description of these results). For our fits with 40 degrees of freedom and 200 bootstrap regions, the expected value of χ^2 is 50.4, not 40. It is clear from the figures that the halo model signal generally is a close match to the data; for example, for early-types, the χ^2 for the fits for the seven stellar mass bins were 37.5, 39.9, 31.5, 36.5, 46.9, 40.5 and 42.0, respectively, with p-values (i.e. the probability to exceed this value by chance if the model is a realistic description of the data) of 0.85, 0.79, 0.96, 0.87, 0.58, 0.78, 0.73. The results may imply that the bootstrap error bars are slight overestimates. Results for late-types in stellar mass bins, and the splits by luminosity, were similar.

One concern regarding these fits is that for the highest stellar mass and luminosity bins the halo model underestimates the signal by a significant amount on small scales ($r < \sim 40\,h^{-1}$ kpc). Because of the sky-subtraction problem (Adelman-McCarthy et al. 2006; M05), only scales $r > 30\,h^{-1}$ kpc are used for the fits even though we have plotted down to $20\,h^{-1}$ kpc, so this discrepancy between the best-fitting and observed signal on these scales does not cause a major increase in the χ^2; however, it is still a concern, since the
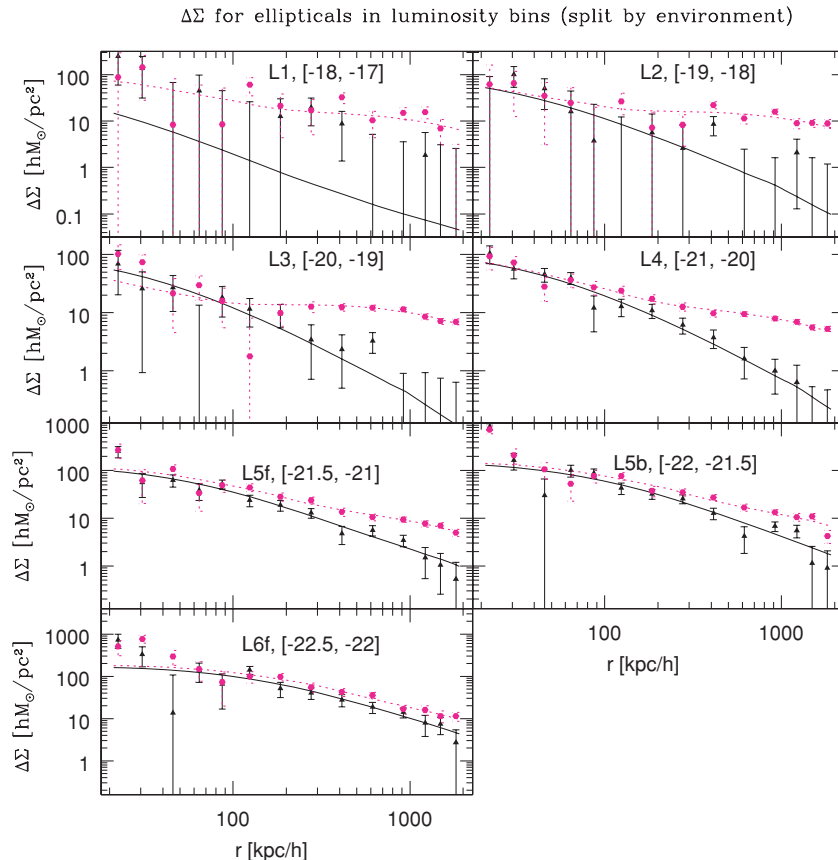
Figure 3. $\Delta\Sigma$ with best-fitting halo model in luminosity bins for early-type galaxies, divided into overdense (magenta hexagons, dashed line) and underdense (black triangles, solid line) samples. All errors are 1σ.

magnitude of the effect is larger than the estimated effect due to sky subtraction (at most 10 per cent). Because the large magnitude of this discrepancy does not seem attributable to any of the small-scale systematics such as intrinsic alignments, the sky-subtraction problem, or magnification bias, the discrepancy seems to suggest a problem with the assumed profile itself, likely due to the effects of stellar component and the associated DM contraction caused by it, which we have completely ignored. A detailed study of this discrepancy between the model and the observed signal will be investigated in the context of DM profile constraints from g–g lensing in future work.

One final issue we must consider is that brought up in Mandelbaum et al. (2005b) of the corrections to the central halo masses due to broadness of the central halo mass distribution, which naturally has some width due to the width of the stellar mass or luminosity bins, and which may be further broadened by scatter in the mass–luminosity (or mass–stellar mass) relationship. As noted there, the best-fitting central halo mass underestimates the mean value (and overestimates the median, which is not of interest in this work) by some amount due to this width. In this work, we use the corrections in the 'no-scatter case' which are purely due to the width of the bins that lead to a wide central halo mass distribution, because we anticipate that our division into early- and late-type samples will lead to narrower central halo mass distributions. Those corrections, as described there, are to increase the best-fitting masses by 6, 11 and 36 per cent for L3, L4 and L5 (1-mag wide), respectively. We extrapolate these values to higher luminosity and use no correction for L1–L2, 6, 11, 25, 50 and 66 per cent for L3, L4, L5f, L5b and L6f,

respectively. Fundamentally, these values are somewhat uncertain, and indeed represent one of the main modelling uncertainties of this paper. All corrections have been applied to values in the tables and text in the following sections. For stellar mass samples, we use the average luminosity of each bin to find a correspondence between stellar mass and luminosity bins, and use corrections of 0, 6, 8, 11, 22, 45 and 66 per cent for stellar mass bins 1–7, respectively. While these corrections introduce some uncertainty in the masses themselves, they do not affect comparisons between morphology samples at the same stellar mass or luminosity since the same corrections are applied to each morphology sample.

4.3 Central halo masses

Here, we present results derived from the best-fitting central halo masses and their 95 per cent confidence intervals. Due to the imposition of the constraint $M_{cent} > 0$, the error distributions at low luminosity and stellar mass are highly non-Gaussian, and the confidence intervals are determined using the distribution of M_{cent} values for the bootstrap subsamples.

First, we consider the relationship between halo mass and stellar mass. Table 3 shows the best-fitting halo mass and its 95 per cent confidence interval as a function of stellar mass for early- and late-type galaxies. For reference, the average r-band luminosity for each sample is also shown. Fig. 4 shows a plot of halo mass as a function of stellar mass, and of central galaxy conversion efficiency as a function of stellar mass, where we define conversion efficiency η via equation (7) with $\Omega_m = 0.27$, $\Omega_b = 0.046$ and $h = 0.7$.

Table 3. The central halo mass determined for stellar mass subsamples separately for early- and late-type galaxies, and the resulting conversion efficiencies determined according to equation (7). All confidence intervals are 95 per cent.

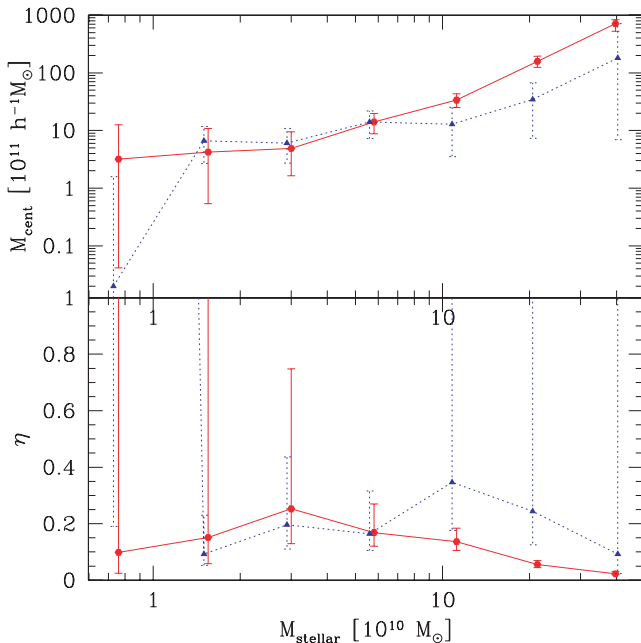| $\langle M_{\rm stellar} \rangle$ $10^{10}\,{\rm M}_\odot$	$M_{\rm cent}$ $10^{11}\,h^{-1}\,{\rm M}_\odot$	η	$\langle L/L_* \rangle$
	Early-types		
0.76	$3.18^{+9.45}_{-3.14}$	$0.098^{+7.44}_{-0.073}$	0.27
1.5	$4.20^{+6.63}_{-3.67}$	$0.15^{+1.00}_{-0.09}$	0.41
3.0	$4.9^{+4.7}_{-3.2}$	$0.25^{+0.50}_{-0.12}$	0.67
5.8	$14.1^{+5.6}_{-5.3}$	$0.17^{+0.10}_{-0.05}$	1.1
11.2	34^{+10}_{-9}	$0.14^{+0.05}_{-0.03}$	1.8
21.3	158^{+37}_{-33}	$0.055^{+0.015}_{-0.010}$	2.9
39.6	716^{+123}_{-190}	$0.023^{+0.008}_{-0.003}$	4.9
	Late-types		
0.73	$0.020^{+1.56}_{-0.018}$	$15.0^{+107}_{-14.8}$	0.38
1.5	$6.6^{+5.1}_{-4.0}$	$0.09^{+0.14}_{-0.04}$	0.63
2.9	$6.1^{+4.7}_{-3.4}$	$0.20^{+0.24}_{-0.09}$	0.77
5.6	14^{+8}_{-7}	$0.16^{+0.15}_{-0.06}$	1.1
10.8	13^{+12}_{-9}	$0.35^{+0.92}_{-0.17}$	1.9
20.5	34^{+33}_{-28}	$0.24^{+0.90}_{-0.12}$	3.2
40.4	180^{+532}_{-173}	$0.09^{+2.32}_{-0.07}$	3.8

Figure 4. Central halo mass (top) and conversion efficiency in central galaxy η (bottom) as a function of stellar mass for early-type (red hexagons, solid line) and late-type (blue triangles, dotted line) galaxies. All error bars shown are 95 per cent confidence interval.

Table 3 and Fig. 4 reveal several interesting trends in the relationship between stellar mass and halo mass. First, stellar mass is a good tracer of halo mass for $M_{\rm stellar} < 10^{11}\,{\rm M}_\odot$ (corresponding roughly to $L < 1.5L_*$); that is, both early- and late-types have the same average relationship between halo and stellar mass in this regime.

Above this value of stellar mass, the central halo mass for early-types is larger than that for late-types. One possible explanation for this trend is that early-types are far more likely to be the central galaxy of a group- or cluster-mass halo than late-types, which are only at the centre of smaller haloes. Thus, the $M_{\rm cent}$ values in this table and figure for early-types at higher values of stellar mass are likely to reflect the mass of the entire group/cluster rather than that of the central galaxy only.

We also consider the lower panel of Fig. 4, the central galaxy conversion efficiency η as a function of $M_{\rm stellar}$. For those bins with a marginal detection of signal, we are able to place only weak constraints on η, which may at times even have a central value outside of the range of reasonable values $0 < \eta < 1$; however, in all cases the 2σ errors shown in the table and figure include part of the range of reasonable values. The particularly useful part of this exercise is the lower limit in η derived from the upper limit on the halo masses. For $M_{\rm stellar} > 10^{11}\,{\rm M}_\odot$, we see a reflection of the trend noted for the early-types in the upper panel, that many of them are central galaxies of groups or clusters, and consequently the interpretation of $M_{\rm stellar}/M_{\rm cent}$ in terms of conversion efficiency is no longer reasonable. (To do so, we would have to include the stellar masses of all other group/cluster members or include the mass of the central galaxy only rather than the full cluster mass.) However, including stellar mass of other group/cluster members would tend to raise η, so while the central value of η is likely to be underestimated at high $M_{\rm stellar}$, the lower limits given here are robust. Hence, for late-type galaxies, we can conclude that for typical galaxies with $M_{\rm stellar} \sim 10^{11}\,{\rm M}_\odot$, the conversion efficiency is typically 35 per cent, with a lower limit of 18 per cent (95 per cent CL). For early-types, the typical galaxy has a conversion efficiency of only 14 per cent, or a lower limit of 11 per cent. These results imply a difference in conversion efficiency between typical early- and late-type galaxies of roughly a factor of 2 or more, with the efficiency for both early- and late-types declining at higher stellar masses.

Next, we consider the relationship between r-band luminosity and halo mass. Table 4 and Fig. 5 give the relevant parameters. This table and figure reveal several interesting points about the relationship between r-band luminosity and halo mass. First, the luminosity is a good tracer of central halo mass for $L < \sim 0.8L_*$, with early- and late-types below this luminosity having consistent halo masses. At higher luminosities, we see a similar trend as for the split by stellar masses, with larger central halo masses at the bright end for early-types, possibly explained by them being at the centres of group- or cluster-mass haloes. Hence, while the relationship between mass and luminosity appears to be consistent with a single power law for late-types, the same is not true for early-types, due to the steepening in this relationship at the bright end (which, in this regime, is more accurately a relationship between the BCG luminosity and the cluster mass rather than an individual galaxy luminosity and mass). In the lower panel of Fig. 5, we note that because of this inclusion of the mass in all group/cluster members, the central values and lower limits of $M_{\rm cent}/L$ are not as relevant as the upper limits. Consistent with the results derived using stellar masses, $M_{\rm cent}/L$ is larger for early-types than for late-types by about a factor of 2 around L_*, and the value of $M_{\rm cent}/L$ decreases significantly for higher luminosities. As for the relationship between halo mass and stellar mass for isolated haloes, we need to use environment estimates to explore what happens to field galaxies at high luminosities in order for the values for early-types to have a simple physical interpretation.

Next, we consider the relationship between local density and halo mass for ellipticals, where we divide each luminosity bin at

Table 4. The central halo mass determined for luminosity subsamples separately for early- and late-type galaxies. All confidence intervals are 95 per cent.

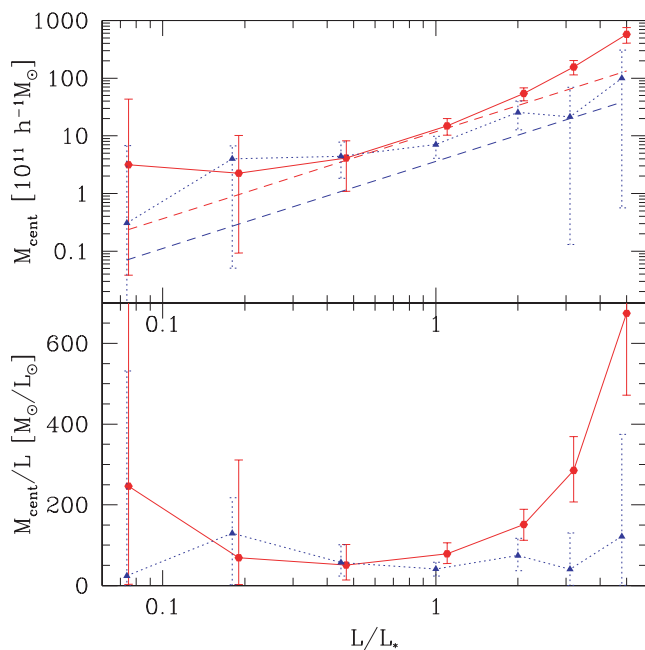| M_r	$\langle L/L_* \rangle$	Early-types		Late-types	
		$M_{\rm cent}$ $10^{11}\,h^{-1}\,{\rm M}_\odot$	$M_{\rm cent}/L$ ${\rm M}_\odot/{\rm L}_\odot$	$M_{\rm cent}$ $10^{11}\,h^{-1}\,{\rm M}_\odot$	$M_{\rm cent}/L$ ${\rm M}_\odot/{\rm L}_\odot$
$[-18, -17)$	0.075	$3.16^{+40}_{-3.13}$	246^{+3113}_{-243}	$0.31^{+6.44}_{-0.30}$	24^{+507}_{-24}
$[-19, -18)$	0.19	$2.2^{+7.9}_{-2.1}$	69^{+242}_{-66}	$4.0^{+2.7}_{-3.9}$	129^{+88}_{-128}
$[-20, -19)$	0.47	$4.1^{+4.1}_{-3.0}$	51^{+51}_{-37}	$4.4^{+3.4}_{-2.6}$	57^{+44}_{-33}
$[-21, -20)$	1.1	$14.9^{+5.0}_{-4.6}$	79^{+27}_{-24}	$7.1^{+2.8}_{-3.0}$	41^{+16}_{-17}
$[-21.5, -21)$	2.1	54 ± 14	151 ± 38	26^{+15}_{-13}	74^{+43}_{-37}
$[-22, -21.5)$	3.2	157^{+46}_{-43}	285^{+83}_{-78}	21^{+48}_{-21}	40^{+90}_{-40}
$[-22.5, -22)$	5.0	578^{+180}_{-174}	674^{+210}_{-203}	100^{+208}_{-100}	122^{+253}_{-121}

Figure 5. Central halo mass (top) and $M_{\rm cent}/L$ as a function of luminosity for early-type (red hexagons, solid line) and late-type (blue triangles, dotted line) galaxies. Dashed lines also show the best-fitting power law $M(L)$ for early- and late-types from Guzik & Seljak (2002) as discussed in the text. All error bars shown are 95 per cent confidence intervals.

Table 5. The central halo mass determined for luminosity subsamples for early-type galaxies in low- and high-density regions separately. All confidence intervals are 95 per cent.

$\langle L/L_* \rangle$	$M_{\rm cent}(10^{11}\,h^{-1}\,{\rm M}_\odot)$ Low density	$M_{\rm cent}(10^{11}\,h^{-1}\,{\rm M}_\odot)$ High density
0.075	$0.66^{+15}_{-0.66}$	$12.0^{+82.8}_{-11.8}$
0.19	$6.3^{+7.6}_{-5.2}$	$5.3^{+11.8}_{-4.8}$
0.47	$7.4^{+5.0}_{-4.9}$	$2.4^{+4.4}_{-1.9}$
1.1	$15.4^{+4.1}_{-5.1}$	15^{+8}_{-6}
2.1	43^{+15}_{-14}	59^{+30}_{-21}
3.2	135^{+41}_{-54}	198^{+109}_{-122}
4.9	443^{+190}_{-222}	725^{+329}_{-599}

depression in the signal relative to that for field galaxies is seen on 50–$100\,h^{-1}$ kpc scales, and therefore we can rule out scenarios that have most satellites strongly stripped.

4.4 Comparison against past studies

Other works have attempted to determine whether haloes of satellite galaxies are tidally stripped. The methodology presented by Natarajan & Kneib (1997) allowed for the mass distributions of individual cluster galaxies to be mapped out, in addition to the large-scale cluster-mass distribution. This method was applied by Natarajan et al. (1998), who found some suggestion that tidal stripping may affect E galaxies less than S0 galaxies (based on differences in velocity dispersions), and Natarajan, Kneib & Smail 2002 (with a longer description of methodology in Natarajan et al. 2004), who found clear evidence for tidal stripping, with field-scale haloes for L_* early-types excluded at the 10σ level. Their density profile for the galaxy-scale haloes differed from the one used in this work, but shares the property that below the truncation radius, $\Delta\Sigma \propto R^{-1}$ (our data is consistent with a power-law index of -0.9, so quite similar), and $\propto R^{-2}$ beyond truncation radius r_t, which is the same as our model, but with the transition happening gradually rather than abruptly as in our model.

For a typical cluster, the truncation radius for L_* early-type galaxies was found in Natarajan et al. (2002) to be 40 kpc or $28\,h^{-1}$ kpc; our best-fitting value of $M_{\rm cent} = 15^{+8}_{-6} \times 10^{11}\,h^{-1}\,{\rm M}_\odot$ for high-density early-type galaxies at $L/L_* = 1.1$ indicates a virial radius of $r = 288\,h^{-1}$ kpc, which combined with the Natarajan et al. (2002)

the median density in that bin. Table 5 and Fig. 6 contain the results.

The signal in Fig. 3, and the best-fitting masses in Table 5 and Fig. 6 appear to suggest that early-type galaxies in both low- and high-density regions have consistent central halo masses, particularly for $L <\sim L_*$ where the high-density sample is exclusively satellites, rather than BCGs. Another interesting point to note is that discussed in Mandelbaum et al. (2005b), that a large amount of tidal stripping of satellite profiles in clusters would cause a clear depression in the lensing signal on scales below the virial radius. For example, a scenario predicted from a combination of N-body simulations with semi-analytic models of galaxy formation suggested by Gao et al. (2004a) is that a very large fraction may have nearly all the DM stripped. (As stated in Section 2, we do assume that all satellites have 50 per cent of the matter stripped.) No such major
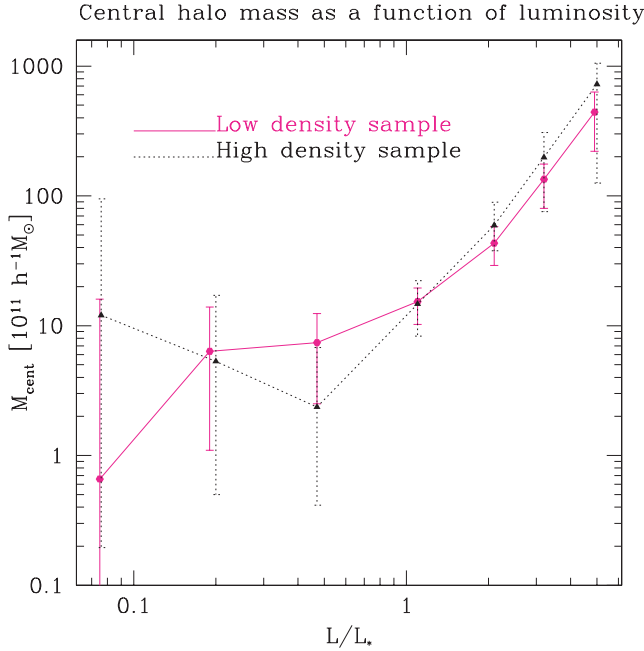
Figure 6. Central halo mass as a function of luminosity for early-type galaxies in low-density (magenta hexagons, solid line) and high-density (black triangles, dotted line) samples. All error bars shown are 95 per cent confidence intervals.

result suggests no DM beyond 10 per cent of the virial radius for an equivalent halo in the field, or 85 per cent of the mass stripped (rather than our assumption of no matter beyond 40 per cent of $r_{\rm vir}$, or half the mass stripped). Tidal stripping beyond $28\,h^{-1}$ kpc would give a much more suppressed signal on scales ~ 28–$200\,h^{-1}$ kpc (above which the group/cluster contribution dominates) than what we see here. However, we note that those results are for a small number of massive clusters (five), whereas our results are an average over all group- and cluster-sized haloes. Furthermore, our results average over all separations from the cluster centre, whereas the results from Natarajan et al. (2002) are all within 50–100 arcsec, or a characteristic scale of $300\,h^{-1}$ kpc, significantly smaller than the virial radius of a massive cluster, and therefore in the regime where the tidal stripping is expected to be more efficient, so it is not possible to draw quantitative conclusions from this comparison. Gavazzi et al. (2004) also found, using a weak lensing analysis of a single supercluster, that for early-types, the typical scale of the DM haloes of satellites decreased from about 300 kpc on the outskirts of clusters to 200 kpc near the cluster cores; this result is consistent with our assumed model of tidal stripping, and with our findings.

A number of previous studies have attempted to determine the relationship between mass and light. Guzik & Seljak (2002) found a roughly power law $M(L) = M_*(L/L_*)^\beta$ in each band using a halo model analysis of g–g weak lensing data in each band from the SDSS, but with a much smaller galaxy sample, and different methods of calibrating the shear and the redshift distributions than are used here. Their results in the r band were $M = (8.96 \pm 1.59) \times 10^{11}\,(L/L_*)^{1.51\pm0.04}\,h^{-1}\,{\rm M_\odot}$, as determined using luminosity samples spanning the range $0.6 < L/L_* < 7$. However, these results assumed $\alpha = 0$; using a more reasonable value of $\alpha \sim 0.2$ gives values of M_* that are 10–20 per cent lower. Furthermore, that work defined the mass using $200\rho_{\rm crit}$ rather than $180\bar\rho$, which means that in order to compare their M_* with ours, we must increase their value of M_* by approximately 30 per cent. Thus, from the combination

of these two effects, we increase their M_* by 10 per cent, yielding $M_* = (9.9 \pm 1.7) \times 10^{11}\,h^{-1}\,{\rm M_\odot}$ (1σ error). In Table 4, we can see that for the luminosity bin closest to L_*, our central halo masses are $(14.9^{+5.0}_{-4.6})$ and $(7.1^{+2.8}_{-3.0}) \times 10^{11}\,h^{-1}\,{\rm M_\odot}$ for early- and late-types, respectively. So, using the 35 per cent spiral fraction for this bin from Table 2, we get an average halo mass of $(12.2^{+2.4}_{-2.5}) \times 10^{11}\,h^{-1}\,{\rm M_\odot}$ (2σ), which is 20 per cent higher than but statistically consistent with the value from Guzik & Seljak (2002). We also compare against their M_* values for early- and late-types in the r band, also corrected upwards by 10 per cent, which are (11.8 ± 2.8) and $(3.6 \pm 2.3) \times 10^{11}\,h^{-1}\,{\rm M_\odot}$ (where the fits allowed α to vary, unlike the above estimates, and fixed β to 1.51), which is also lower than but consistent with our results. In Fig. 5, the top panel includes as dashed lines the $M(L)$ for early- and late-types from Guzik & Seljak (2002); as shown, the fit, while not perfect, is not totally ruled out by our 2σ errors. In particular, for late-types, the slope appears reasonable but the amplitude slightly low compared to our results, whereas for early-types, the deviation between our results and the fits is most prominent for high luminosities, where the fits underestimate $M_{\rm cent}$ (i.e. our results are consistent with a steeper slope β). We note that there are a number of other differences in the modelling between this paper and that one (e.g. the determination of α and a lack of corrections for width of the central halo mass distribution in the older work), and differences in calibration of the lensing signal, so a more detailed comparison is not necessarily useful or meaningful.

Next, we compare against the recent work by Hoekstra et al. (2005). A number of factors make direct comparison difficult: the different average lens redshift (with complications due to luminosity evolution), the use of different passbands (V, B and R rather than SDSS bands), the different definitions of virial mass and the selection of only isolated galaxies to avoid the need to fit for a non-central term. However, a number of their findings may be compared directly against ours. First, they find $M \propto L^{1.5}$ in all three bands, similar to Guzik & Seljak (2002); the previous paragraph includes a discussion of this result relative to ours as shown in Fig. 5. Next, when accounting for luminosity evolution, difference in passbands and different definitions of mass, Hoekstra et al. (2005) find that their masses are about 25 per cent higher than those from Guzik & Seljak (2002) when comparing against the g-band results, but still statistically consistent. This result implies that our results for the masses are consistent with those from Hoekstra et al. (2005), since our masses are also slightly higher than those from Guzik & Seljak (2002). Finally, Hoekstra et al. (2005) find conversion efficiencies a factor of 2 higher for late-types than for early-types, 33 per cent versus 14 per cent. This difference in morphology appears to be consistent with our results (see Fig. 4) for stellar masses larger than $10^{11}\,{\rm M_\odot}$ or $L \gtrsim L_*$; for lower stellar masses or luminosities, we lack statistical precision to make concrete statements.

The conditional luminosity function fits to 2dF data from van den Bosch et al. (2003) yield $M(L)$ that is quite similar to that given in Vale & Ostriker (2004) based on empirical models, which is $M \propto L^{0.25}$ at low mass (or luminosity), and $M \propto L^{3.6}$ at the high-mass end, where the luminosity is that of the BCG alone (i.e. not all the cluster galaxies combined) and the mass is that of the full cluster. While we are unable to constrain the power-law slope very well at low luminosities because of the errors, the three brightest luminosity bins with (L5f, L5b, L6f) give $M \propto L^{2.7\pm0.6}$ (95 per cent CL), with exponent about 3σ below the Vale & Ostriker (2004) model predictions. Fig. 1 from van den Bosch, Yang & Mo (2004) also shows that the conversion efficiency is highest for L_* galaxies, with rapidly increasing M/L for lower and higher masses, consistent with our results.

Analytical models of the Milky Way (Klypin, Zhao & Somerville 2002) predict halo masses of $7 \times 10^{11}\, h^{-1}\, M_\odot$, where the mass is defined as that within the radius within which the average density is equal to $340\overline{\rho}$. To compare against our results, their mass estimate must be increased by 15 per cent, giving $8 \times 10^{11}\, h^{-1}\, M_\odot$, which we compare against our result for L_* late-type galaxies, $M_{\text{cent}} = (7.1^{+2.8}_{-3.0}) \times 10^{11}\, h^{-1}\, M_\odot$ (95 per cent CL). Alternatively, we note that their table 2 suggests a total stellar mass of $6 \times 10^{10}\, M_\odot$, which is typical of L_* galaxies and which (according to our Table 3) gives a halo mass of $M_{\text{cent}} = 14^{+8}_{-7} \times 10^{11}\, h^{-1}\, M_\odot$. Thus, it appears that this analytical model of the Milky Way is consistent with our results at the 95 per cent CL.

It is also worthwhile to compare against the lensing signal from N-body simulations. In this case, we compare against the fit results from Mandelbaum et al. (2005b), which showed the lensing signal for three luminosity bins from simulations described in Tasitsiomi et al. (2004), both with and without scatter in the mass–luminosity relationship: L3, L4 and L5 (a bin 1-mag wide that includes L5f and L5b). Without scatter, the values of M_{cent} (mean) in each bin were 5.1, 18 and $132 \times 10^{11}\, h^{-1}\, M_\odot$; with scatter, they were 7.5, 29 and $117 \times 10^{11}\, h^{-1}\, M_\odot$. For this paper, if we combine the results in each bin (averaging the results with different morphologies using the spiral fraction for weighting purposes), we get 4.3 ± 2.5, 12 ± 3 and $(82 \pm 15) \times 10^{11}\, h^{-1}\, M_\odot$. Therefore, the results from simulations seem to give somewhat higher masses than are found in the real data, though just within the 95 per cent confidence intervals, except for L5.

Finally, we compare against the baryonic mass function determination by Read & Trentham (2005) that uses a variety of data sources. In that work, the fraction of baryons in galaxies is estimated to be ∼10 per cent, and of those, ∼80 per cent are in stars (with the star formation efficiency varying by morphological type). Hence, the results from Read & Trentham (2005) suggest average η values of 0.08. While our peak values of η (around $10^{11}\, h^{-1}\, M_\odot$) are higher than this, the abundance of galaxies at much lower stellar mass (for which our central values of η are lower but poorly constrained) suggests that our results and those of Read & Trentham (2005) are consistent within the errors. Furthermore, their results and ours both suggest the trend of decreasing η with increasing stellar mass above $10^{11}\, h^{-1}\, M_\odot$. They attribute this trend to feedback from active galactic nuclei which would tend to lower the baryonic fraction in high-mass galaxies (e.g. Silk & Rees 1998).
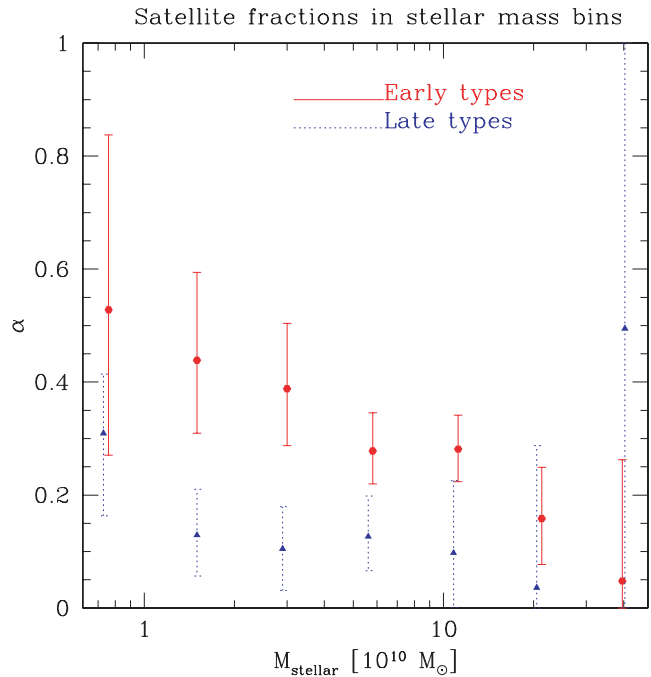

Figure 7. Satellite fractions as a function of stellar masses for samples split into early (red hexagons, solid lines) versus late (blue triangles, dotted lines) types. Error bars shown are 95 per cent confidence intervals.

Table 7. The satellite fraction determined for luminosity subsamples separately for early- and late-type galaxies, and for early-type galaxies split into low-density and high-density samples. All confidence intervals are 95 per cent.

$\langle L/L_* \rangle$	α Early-types (all)	α Late-types (all)	α Early-types (low density)	α Early-types (high density)
0.075	$0.54^{+0.39}_{-0.40}$	$0.15^{+0.22}_{-0.15}$	$0.006^{+0.24}_{-0.006}$	$0.81^{+0.19}_{-0.57}$
0.19	$0.52^{+0.25}_{-0.21}$	$0.19^{+0.17}_{-0.08}$	$(1.2^{+442}_{-1.1}) \times 10^{-4}$	$1.00^{+0.00}_{-0.24}$
0.47	$0.44^{+0.13}_{-0.10}$	$0.14^{+0.07}_{-0.06}$	$(3.1^{+6376}_{-1.9}) \times 10^{-5}$	$0.96^{+0.04}_{-0.20}$
1.1	$0.27^{+0.06}_{-0.05}$	$0.13^{+0.05}_{-0.05}$	$(9.3^{+5079}_{-8.5}) \times 10^{-5}$	$0.55^{+0.12}_{-0.10}$
2.1	$0.17^{+0.08}_{-0.06}$	$(2.2^{+804}_{-2.1}) \times 10^{-4}$	$0.046^{+0.087}_{-0.046}$	$0.43^{+0.12}_{-0.15}$
3.2	$0.24^{+0.12}_{-0.09}$	$0.18^{+0.38}_{-0.18}$	$0.03^{+0.15}_{-0.03}$	$0.38^{+0.39}_{-0.21}$
4.9	$0.15^{+0.26}_{-0.15}$	$0.0017^{+0.92}_{-0.0016}$	$0.07^{+0.28}_{-0.07}$	$0.19^{+0.81}_{-0.19}$

4.5 Satellite fractions

Here, we present results for the satellite fractions as a function of luminosity, stellar mass and morphology. Table 6 and Fig. 7 show the best-fitting α in stellar mass bins with 95 per cent confidence intervals from the bootstrap, for early- and late-types separately. Table 7 shows the best-fitting value of α in luminosity bins with 95 per cent confidence intervals, for early- and late-types, and for early-types split by local density, and Fig. 8 shows these results as well. We note that M_{cent} and α have a cross-correlation coefficient of about -0.7 from the fits, because the choice of M_{cent} determines the mass at which $\langle N(M) \rangle$ becomes proportional to M, which has a significant effect on the satellite contribution.

Table 6. The satellite fraction determined for stellar mass subsamples separately for early- and late-type galaxies. All confidence intervals are 95 per cent.

$\langle M_{\text{stellar}} \rangle$ $(10^{10}\, M_\odot)$	α Early-types	α Late-types
0.76	$0.53^{+0.31}_{-0.26}$	$0.31^{+0.10}_{-0.15}$
1.5	$0.44^{+0.16}_{-0.13}$	$0.13^{+0.08}_{-0.07}$
3.0	$0.39^{+0.12}_{-0.10}$	$0.10^{+0.07}_{-0.07}$
5.7	$0.28^{+0.07}_{-0.06}$	$0.13^{+0.07}_{-0.06}$
11.1	$0.28^{+0.06}_{-0.06}$	$0.10^{+0.13}_{-0.10}$
21.0	$0.16^{+0.09}_{-0.08}$	$0.04^{+0.25}_{-0.04}$
40.0	$0.05^{+0.21}_{-0.05}$	$0.47^{+0.53}_{-0.47}$

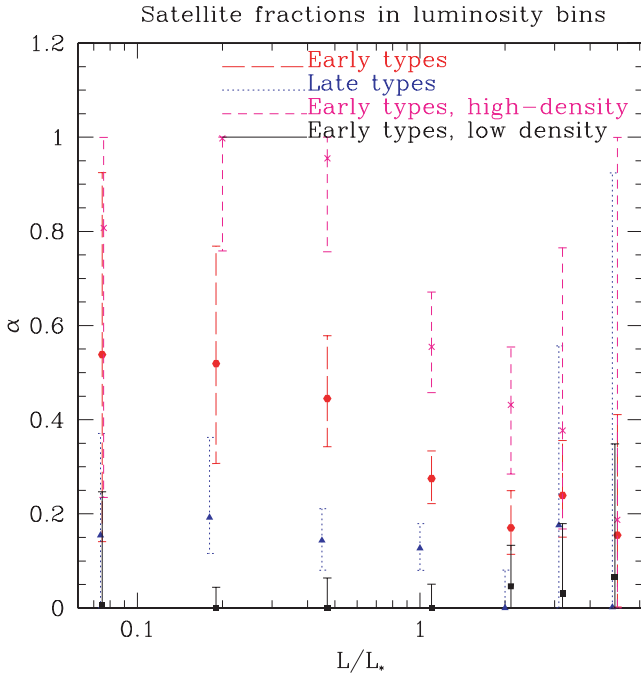Satellite fractions in luminosity bins

Figure 8. Satellite fractions as a function of luminosity for samples split into early (red hexagons, long-dashed lines) versus late (blue triangles, dotted lines) types, and early types split into high-density (magenta crosses, dashed lines) and low-density (black squares, solid lines) samples. Error bars shown are 95 per cent confidence intervals.

We discuss both Figs 7 and 8 together. For both the splits by luminosity and by stellar mass, the trend is for α for early-types to decrease slightly with L or $M_{\rm stellar}$, with central values around 0.5 at $M_{\rm stellar} \sim 0.8 \times 10^{10}$ M$_\odot$ or $L/L_* \sim 0.1$, decreasing to a central value of 0.1 (upper limit $\sim$0.2) for $M_{\rm stellar} \geqslant 20 \times 10^{10}$ M$_\odot$, or 0.2 (upper limit $\sim$0.35) for $L/L_* > 2$. We remind the reader that these numbers do not limit the number of early-type lenses that are in groups and clusters, because a galaxy that is the BCG of a group/cluster (of which we expect many in L5 and L6) will *not* be included as a satellite. Hence, it is possible that the number of early-type galaxies in groups or clusters is actually constant with L or $M_{\rm stellar}$ when the number that are BCGs is accounted for; unfortunately, we cannot test this hypothesis using our halo model formalism.

For early-types, we also have done a simultaneous split by luminosity and density. As shown, for $L/L_* < \sim 2$, this split seems to do an excellent job of isolating those early-type galaxies that are in groups and clusters. For example, for L3 ($L/L_* \sim 0.5$), we see that the central value of α for the full sample of early-type galaxies is 0.44, for the low-density elliptical sample is consistent with zero, and for the high-density elliptical sample is 0.96. Since the low- and high-density samples are determined by splitting at the median environment estimate, these results for satellite fractions are fully consistent with each other. For all luminosity bins, similar consistency relationships are satisfied within the noise. We expect that for higher luminosities, many of the high-density sample are BCGs of groups and clusters, which may account for the discrepancy noted in central halo masses in the previous section, and for the decline of satellite fraction with luminosity for this sample.

For late-types, there is no suggestion of a statistically significant change in the group/cluster fraction with luminosity or stellar mass, with central values $\sim$0.10–0.15 and upper bounds typically

0.25–0.3. The lower satellite fraction for late-types than for early-types is consistent with works cited previously.

The overall trend of satellite fraction decreasing with mass is also observed with simulations and semi-analytic galaxy formation models of Zheng et al. (2004).

We compare these results against derived satellite fractions from Zehavi et al. (2005) for L2, L3 and L4. They find that 10–30 per cent of blue galaxies are satellites independent of luminosity, consistent with our results. Of the red galaxies, they find satellite fractions of 0.72, 0.54, 0.35 for L2, L3 and L4, respectively, so the trend of α decreasing with luminosity is found in both their autocorrelation analysis and our lensing analysis. However, our values of α for these bins are $0.52^{+0.25}_{-0.21}$, $0.44^{+0.13}_{-0.10}$ and $0.27^{+0.06}_{-0.05}$, about 30 per cent lower than their results, though for L2 and L3 their values of α lie within our 95 per cent confidence intervals; for L4, they lie slightly outside our 95 per cent intervals, but when the errors on their estimates are included, it is not clear that the discrepancy is significant. They also find that the average host halo mass for L2 galaxies (i.e. the mass of the full cluster if they are in a cluster, or the halo mass of field galaxies, which are in the minority) is $2.5 \times 10^{14} \, h^{-1}$ M$_\odot$. We have found (Mandelbaum et al. 2005b) that the lensing signal on group and cluster scales is actually dominated by less massive haloes, in the mass range 10^{13}–10^{14}; if the average host halo mass was as high as the value given in Zehavi et al. (2005), then considering the large satellite fraction in this bin, the lensing signal would be too large to be consistent with observations on $500 \, h^{-1}$ kpc–$1 \, h^{-1}$ Mpc scales (increasing by more than a factor of 2 from its current value).

4.6 Robustness of best-fitting parameters

In order to determine the robustness of these results, we consider which modelling assumptions may affect them. The first effect we consider is that of $\langle N(M) \rangle$ which has been modelled here as a power law $\langle N(M) \rangle \propto M$ for $M > 3M_{\rm cent}$ and $\propto M^2$ for $M < 3M_{\rm cent}$, so $3M_{\rm cent}$ marks the point below which it falls off rapidly. This choice was justified in Section 2, but we must consider the effects of this choice on our results for the best-fitting satellite fractions. In particular, in Mandelbaum et al. (2005b), we found that the power-law exponent ϵ of $\langle N(M) \rangle$ for $M > 3M_{\rm cent}$ was almost completely degenerate with α. The two parameters essentially arranged themselves to preserve the amount of signal coming from haloes in the mass range 10^{13}–$10^{14} \, h^{-1}$ M$_\odot$ (higher-mass haloes are not important because they are killed off by the exponential in the mass function dn/dM, and lower-mass haloes do not contribute a significant amount of signal). Thus, our satellite fractions have the potential to differ significantly from the real one if ϵ is incorrect.

van den Bosch et al. (2003) find using data from 2dF Galaxy Redshift Survey (Colless et al. 2001, 2dFGRS) that $\langle N(M) \rangle$ has a different power-law dependence for spirals (shallower) and ellipticals (steeper), with the net result being that the bright luminosity bins, which are dominated by ellipticals, show a single power law, but fainter luminosity bins are best described by a combination of the two power laws, with the spiral one dominating at low mass and the elliptical one dominating at high mass. This finding is reasonable in light of the fact that spirals are known to dominate in the field and ellipticals in clusters. However, it does mean that our assumption of $\epsilon = 1$ for both early- and late-types may complicate our analysis, since it may have caused an overestimate of α for early-types and underestimate for late-types, which is exactly in the direction of the difference we measured (i.e. lower satellite fractions for late-types).

As noted in van den Bosch et al. (2003), which seems to suggest $\epsilon \sim 0.8$ for ellipticals and $\sim$0.6 for spirals using the 2dFGRS

b_J-band data (in agreement with another b_J-band study using Automated Plate Measuring Machine (APM) data, Scoccimarro et al. 2001, which found $\epsilon \sim 0.8$ overall), we do not expect ϵ to be the same when determined using data selected by absolute luminosity in different bands, so in order to estimate its value for early- and late-types and its possible luminosity evolution, we turn to Zehavi et al. (2005), which uses SDSS samples selected in the r band and a halo model analysis of $\xi_{gg}(r_p)$ in order to determine this parameter.[1] The right-hand side of fig. 18 in that paper shows the best-fitting value of ϵ for samples selected by luminosity *thresholds* rather than 1-mag wide bins; as shown, the value of ϵ is ~ 0.9 for $M_r < -18$ samples, rising slowly to $\epsilon \sim 1.3$ for $M_r < -20.5$ samples, then rising sharply to $\epsilon \sim 2$ above that. This trend may reflect the relatively higher fraction of early-types in the brighter luminosity-threshold samples. The lower right-hand panel of their fig. 22 shows the best-fitting $\langle N(M) \rangle$ for early- and late-types, from which we deduce values of $\epsilon \sim 1.65$ and 1.10, respectively. We note that Zheng et al. (2004), on the other hand, find $\epsilon \sim 1$ for all samples with the same data, reflecting a difference in the modelling. The difference may be attributed to the fact that Zehavi et al. (2005) lack a lower mass cut-off for their $\langle N(M) \rangle$, whereas this work and Zheng et al. (2004) do include a lower-mass cut-off. Because of the lack of cut-off in Zehavi et al. (2005), their value of ϵ must necessarily be quite high for the brightest samples in order to limit the contribution from lower-mass haloes. We note that Conroy, Wechsler & Kravtsov (2005) have explicitly tested this hypothesis by fitting for ϵ with and without a lower mass cut-off, and found that the lack of lower-mass cut-off can increase the best-fitting ϵ by as much as 50 per cent.

We consider the effect of changing ϵ on the best-fitting values of α for early- and late-types separately by calculating an analytic correction assuming the Zehavi et al. (2005) values of ϵ for those samples independent of luminosity or stellar mass; this correction requires that we compute the non-central lensing signal for satellites residing in 10^{13}–$10^{14}\,h^{-1}\,M_\odot$ haloes as the product of α times an integral involving $\langle N(M) \rangle$, and requiring that it be preserved when we change ϵ, thus telling us the new value of α as well. We note that the correction factor is a function of central halo mass because, for high values of central halo mass, the cut-off $3M_{cent}$ will be within our mass range of interest, so changing ϵ will have less of an effect. For both stellar mass and luminosity bins, the results of this calculation indicate that for late-types, changing ϵ from our assumed value of 1.0 to the Zehavi et al. (2005) value of 1.1 requires that we decrease α by 4 per cent of its best-fitting value, which is significantly less than the statistical error on this value for any stellar mass bin. For stellar mass samples, for early-types, changing ϵ from 1.0 to 1.65 requires that we decrease α by 21 per cent of its original value for the five lowest stellar mass bins, 12 per cent for sm6 and no decrease for the largest stellar mass bin (due to its high central halo mass). For luminosity samples, for early-types, it is to decrease α by 21 per cent for the five lowest bins ($-17 \geqslant M_r > -21.5$), by 12 per cent for $-21.5 \geqslant M_r > -22$, and no decrease for $-22 \geqslant M_r > -22.5$. Thus, the value of α for late-types is nearly unchanged, and for early-types, the limiting value at lower stellar mass becomes 0.4 rather than 0.5. We note that for the split by environment, since we only use early-types, the same correction factors apply as for the full early-type sample, so while the actual values of α must be lowered, this correction does not affect the consistency relationship between

the satellite fractions in the low- and high-density early-type samples relative to the full early-type samples. Finally, we remind the reader that since the Zehavi et al. (2005) values of ϵ are higher than our assumed value in part due to a significant difference in modelling, and such high values of ϵ are not consistent with N-body simulation results when using a model similar to ours, these corrections are actually quite conservative.

Next, we consider the fact that the expected signal depends on the radial distribution of satellites within groups and clusters. As mentioned in Section 2, this distribution is not well known, and is assumed here to be an NFW profile with the same concentration parameter as the DM. Variations in c_g cause the non-central signal to peak at different characteristic radii as shown in Guzik & Seljak (2002), thus affecting primarily the shape of the signal rather than its amplitude. Unfortunately, since in most cases the values of α are ~ 0.2–0.3, we are not highly sensitive to c_g and cannot place much of a constraint on it.

Several observational results have suggested that within clusters, red galaxies are more centrally concentrated than blue ones (Oemler 1974; Melnick & Sargent 1977; Dressler 1980; Adami, Biviano & Mazure 1998). Due to a relatively low sensitivity to c_g, we do not fit for it, but see what happens to the fit χ^2 and to the best-fitting M_{cent} and α if we use $c_g = 2c_{DM} \sim 24$ for early-types, and $c_g = 0.5c_{DM} \sim 6$ for late-types. We do this comparison only for L3, L4, L5f and L5b, since these are the samples with the greatest statistical power.

For early-types, we find that because increasing c_g moves the non-central contribution of the signal to relatively small scales, this change actually affects the central halo mass M_{cent} more than it affects the satellite fraction, with the tendency being to decrease the halo mass slightly to compensate for the higher non-central signal on ~ 100–$200\,h^{-1}$ kpc scales. This change only affects the best-fitting χ^2 by ~ 1, with the change being in different directions for the different luminosity bins. The masses in L3, L4, L5f and L5b decrease to 60, 59, 87 and 86 per cent of their values from the fits with $c_g = c_{DM}$, and the satellite fraction changes by -0.01, -0.02, -0.01 and -0.01 (absolute value, not per cent of original). Hence, the changes to α for early-types are well within the statistical error bars, and we conclude that best-fitting values are relatively robust to uncertainties in c_g. The changes to the best-fitting values of M_{cent} are at most 1σ (for L3) and usually somewhat less than that, and thus we conclude that this parameter is also not sensitive to changes in c_g within our statistical error bars, though with more data this statement may no longer be true.

For late-types, the decrease from $c_g = c_{DM}$ to $c_g = 0.5c_{DM}$ decreased the best-fitting χ^2 by at most 1, and had less of an effect on the best-fitting M_{cent} because it shifted the non-central contribution to higher radius. The masses in L3, L4, L5f and L5b increased by 9, 5, 1 and 15 per cent of their original values, well within the 1σ errors, and α increased by 0.02, 0.02, 0.00 and 0.00, also well within the errors. We thus conclude that uncertainty in the distribution of satellites within groups and clusters is not a significant source of systematic uncertainty in our estimates of satellite fractions and central halo masses.

Another source of uncertainty in these estimates is our modelling of the h–h term, which affects the signal on large scales, and thus can change the best-fitting α and (through their degeneracy) M_{cent}. Fortunately, since the h–h term is small on $r < 2\,h^{-1}$ Mpc scales, we find that neglecting it entirely changes the best-fitting parameters by less than 1σ.

Finally, we remind the reader that due to the assumption of a universal IMF when deriving stellar mass estimates, these estimates

---

[1] Note that both Zehavi et al. (2005) and Zheng et al. (2004) call this parameter α (i.e. the symbol we use for the satellite fraction), rather than ϵ.

may need to be rescaled by a constant factor of up to 30 per cent (conservatively). The main results that are affected by this rescaling are the limits that we have placed on conversion efficiencies. All other mass-related results, such as trends in halo masses with stellar mass, and comparisons between different morphology or density samples at constant stellar mass, are unaffected.

5 CONCLUSIONS

In this work, we have used halo model analysis of the g–g weak lensing signal in order to observe trends in the relationship between stellar masses and halo masses, and luminosity and halo mass, treating samples based on morphology separately. We have also studied ellipticals in low- and high-density regions separately.

As a result, we have come to a number of conclusions related to average halo masses. First, the $M_{stellar}/M_{cent}$ ratio is highest for $M_{stellar} \sim 10^{11}$ M$_\odot$, with a peak conversion efficiency of roughly 14 per cent for ellipticals (>11 per cent at 95 per cent CL, statistical error only), although we cannot exclude even larger values at low luminosity or stellar mass where the lensing signal is weak. The corresponding number for spirals reaches 35 per cent at the maximum, but with a larger measurement error, which allows it to be as low as 18 per cent (95 per cent CL). These results imply a factor of 2 or more difference in conversion efficiency between typical spirals and ellipticals above stellar mass of 10^{11} M$_\odot$, whereas below this stellar mass, we find no inconsistency between the conversion efficiencies of early- and late-types, implying that stellar mass is a good tracer of halo mass in this regime. Note that since we are only including central galaxy stellar mass in the analysis, our conversion efficiencies should be viewed as lower limits, and also serve as lower limits on star formation efficiency. In practice, for a 10^{12} M$_\odot$ halo, the central galaxy likely contains most of the stars and the contribution from satellites is negligible, while for a 10^{15} M$_\odot$ halo other galaxies outside the halo centre contribute significantly to the total stellar content of a cluster. Thus, while the upper limits to the conversion efficiency are uncertain both because of large observational errors and because of modelling uncertainties, a lower limit of about 10 per cent (95 per cent CL) is robust for both spirals and ellipticals. Similarly, M/L reaches a minimum for $L \sim L_*$ galaxies of 41^{+16}_{-17} M$_\odot$/L$_\odot$ for late-types, or for $L \sim L_*/2$ of 51^{+51}_{-37} for early-types (95 per cent CL). Below these values of stellar mass (with peak ξ) or luminosity (with minimum M/L) both of those quantities trace halo mass well, meaning that halo masses for early- and late-types were consistent. At higher stellar mass or luminosity, the early-types have a larger central halo mass, likely reflecting the fact that they tend to reside at the centre of clusters, unlike late-types.

We also have a number of conclusions regarding satellite fractions. The satellite fraction for late-types tends to be 10–15 per cent regardless of luminosity. For early-types, the situation is more complex, with a satellite fraction of ∼40–50 per cent at low luminosity, decreasing to about 20 per cent at high luminosity. These trends are consistent with those based on autocorrelation analysis (Zehavi et al. 2005), though the actual values of satellite fraction for early-types are slightly different, possibly reflecting differences in modelling. Our fit results for $L < \sim L_*$ early-types indicate that our density estimate is highly efficient at isolating a nearly pure satellite sample in this regime, which can then be used in a future work that will study tidal stripping and the radial distribution of satellites within groups and clusters. Current results suggest that tidal stripping is not completely efficient in removing the DM from the satellites, since the satellite sample shows plenty of lensing signal at small (50–100 h^{-1} kpc) scales.

REFERENCES

Abazajian K. et al., 2003, AJ, 126, 2081
Abazajian K. et al., 2004, AJ, 128, 502
Abazajian K. et al., 2005, AJ, 129, 1755
Adami C., Biviano A., Mazure A., 1998, A&A, 331, 439
Adelman-McCarthy J. K. et al., 2006, ApJS, 162, 38
Balogh M. L., Schade D., Morris S. L., Yee H. K. C., Carlberg R. G., Ellingson E., 1998, ApJ, 504, L75+
Balogh M. L., Morris S. L., Yee H. K. C., Carlberg R. G., Ellingson E., 1999, ApJ, 527, 54
Balogh M. L., Baldry I. K., Nichol R., Miller C., Bower R., Glazebrook K., 2004a, ApJ, 615, L101
Balogh M. et al., 2004b, MNRAS, 348, 1355
Bernstein G. M., Jarvis M., 2002, AJ, 123, 583
Blanton M. R., Eisenstein D. J., Hogg D. W., Schlegel D. J. S., Brinkmann J., Quintero A. D., Berlind A., Wherry N., 2003a, Am. Astron. Soc. Meeting Abstr., 203, 20314501
Blanton M. R., Lin H., Lupton R. H., Maley F. M., Young N., Zehavi I., Loveday J., 2003b, AJ, 125, 2276
Blanton M. R. et al., 2003c, AJ, 125, 2348
Blanton M. R. et al., 2005a, AJ, 129, 2562
Blanton M. R., Eisenstein D., Hogg D. W., Schlegel D. J., Brinkmann J., 2005b, ApJ, 629, 143
Brainerd T. G., Blandford R. D., Smail I., 1996, ApJ, 466, 623
Bruzual G., Charlot S., 2003, MNRAS, 344, 1000
Bullock J. S., Kolatt T. S., Sigad Y., Somerville R. S., Kravtsov A. V., Klypin A. A., Primack J. R., Dekel A., 2001, MNRAS, 321, 559
Cappellari M. et al., 2006, MNRAS, 366, 1126
Carlberg R. G., Yee H. K. C., Ellingson E., 1997, ApJ, 478, 462+
Carlberg R. G., Yee H. K. C., Morris S. L., Lin H., Hall P. B., Patton D. R., Sawicki M., Shepherd C. W., 2001, ApJ, 563, 736
Coil A. L. et al., 2004, ApJ, 609, 525
Colless M. et al., 2001, MNRAS, 328, 1039
Conroy C., Wechsler R. H., Kravtsov A. V., 2005, preprint (astro-ph/0512234)
Cooray A., 2006, MNRAS, 365, 842
Cooray A., Sheth R., 2002, Phys. Rep., 372, 1
Cooper M. C., Newman J. A., Madgwick D. S., Gerke B. F., Yan R., Davis M., 2005, ApJ, 634, 833
Croton D. J. et al., 2005, MNRAS, 356, 1155
Davis M., Geller M. J., 1976, ApJ, 208, 13

Davis M. et al., 2003, Proc. SPIE, 4834, 161

Davis M., Gerke B. F., Newman J. A., 2004, preprint (astro-ph/0408344)

Dressler A., 1980, ApJ, 236, 351

Eisenstein D. J. et al., 2001, AJ, 122, 2267

Eke V. R., Navarro J. F., Steinmetz M., 2001, ApJ, 554, 114

Finkbeiner D. P. et al., 2004, AJ, 128, 2577

Fischer P. et al., 2000, AJ, 120, 1198

Fukugita M., Ichikawa T., Gunn J. E., Doi M., Shimasaku K., Schneider D. P., 1996, AJ, 111, 1748

Gao L., De Lucia G., White S. D. M., Jenkins A., 2004a, MNRAS, 352, L1

Gao L., White S. D. M., Jenkins A., Stoehr F., Springel V., 2004b, MNRAS, 355, 819

Gao L., Springel V., White S. D. M., 2005, MNRAS, 363, L66

Gavazzi R., Mellier Y., Fort B., Cuillandre J.-C., Dantel-Fort M., 2004, A&A, 422, 407

Gunn J. E. et al., 1998, AJ, 116, 3040

Gunn J. E. et al. 2006, AJ, in press (astro-ph/0602326)

Guzik J., Seljak U., 2001, MNRAS, 321, 439

Guzik J., Seljak U., 2002, MNRAS, 335, 311

Hirata C., Seljak U., 2003, MNRAS, 343, 459

Hirata C. M. et al., 2004, MNRAS, 353, 529

Hoekstra H., Franx M., Kuijken K., Carlberg R. G., Yee H. K. C., 2003, MNRAS, 340, 609

Hoekstra H., Yee H. K. C., Gladders M. D., 2004, ApJ, 606, 67

Hoekstra H., Hsieh B. C., Yee H. K. C., Lin H., Gladders M. D., 2005, ApJ, 635, 73

Hogg D. W., Finkbeiner D. P., Schlegel D. J., Gunn J. E., 2001, AJ, 122, 2129

Hogg D. W. et al., 2003, ApJ, 585, L5

Hogg D. W. et al., 2004, ApJ, 601, L29

Hansen S. M., McKay T. A., Wechsler R. H., Annis J., Sheldon E. S., Kimball A., 2005, ApJ, 633, 122

Hudson M. J., Gwyn S. D. J., Dahle H., Kaiser N., 1998, ApJ, 503, 531+

Ivezić Ž. et al., 2004, Astronomische Nachrichten, 325, 583

Jing Y. P., Mo H. J., Boerner G., 1998, ApJ, 494, 1+

Kaiser N., Squires G., Broadhurst T., 1995, ApJ, 449, 460

Kauffmann G., Colberg J. M., Diaferio A., White S. D. M., 1999, MNRAS, 303, 188

Kauffmann G. et al., 2003, MNRAS, 341, 33

Klypin A., Zhao H., Somerville R. S., 2002, ApJ, 573, 597

Kravtsov A. V., Berlind A. A., Wechsler R. H., Klypin A. A., Gottlöber S., Allgood B., Primack J. R., 2004, ApJ, 609, 35

Kroupa P., 2001, MNRAS, 322, 231

Lin Y., Mohr J. J., Stanford S. A., 2004, ApJ, 610, 745

Lupton R. H., Gunn J. E., Ivezić Z., Knapp G. R., Kent S., Yasuda N., 2001, in ASP Conf. Ser. Vol. 238, Astronomical Data Analysis Software and Systems X. Astron. Soc. Pac., San Francisco, p. 269

Madgwick D. S. et al., 2003, ApJ, 599, 997

Mandelbaum R. et al., 2005a, MNRAS, 361, 1287 (M05)

Mandelbaum R., Tasitsiomi A., Seljak U., Kravtsov A. V., Wechsler R. H., 2005b, MNRAS, 362, 1451

Marinoni C., Davis M., Newman J. A., Coil A. L., 2002, ApJ, 580, 122

McKay T. A. et al., 2001, preprint (astro-ph/0108013)

Melnick J., Sargent W. L. W., 1977, ApJ, 215, 401

Nagai D., Kravtsov A. V., 2005, ApJ, 618, 557

Natarajan P., Kneib J.-P., 1997, MNRAS, 287, 833

Natarajan P., Kneib J.-P., Smail I., Ellis R. S., 1998, ApJ, 499, 600

Natarajan P., Kneib J.-P., Smail I., 2002, ApJ, 580, L11

Natarajan P., Kneib J.-P., Smail I., Ellis R., 2004, preprint (astro-ph/0411426)

Navarro J. F., Frenk C. S., White S. D. M., 1996, ApJ, 462, 563+

Oemler A. J., 1974, ApJ, 194, 1

Padmanabhan N. et al., 2005, MNRAS, 359, 237

Peacock J. A., Smith R. E., 2000, MNRAS, 318, 1144

Pier J. R., Munn J. A., Hindsley R. B., Hennessy G. S., Kent S. M., Lupton R. H., Ivezić Ž., 2003, AJ, 125, 1559

Postman M., Geller M. J., 1984, ApJ, 281, 95

Ramella M., Boschin W., Fadda D., Nonino M., 2001, A&A, 368, 776

Read J. I., Trentham N., 2005, RSPTA, 363, 2693

Richards G. T. et al., 2002, AJ, 123, 2945

Schlegel D. J., Finkbeiner D. P., Davis M., 1998, ApJ, 500, 525

Scoccimarro R., Sheth R. K., Hui L., Jain B., 2001, ApJ, 546, 20

Seljak U., 2000, MNRAS, 318, 203

Seljak U., Warren M. S., 2004, MNRAS, 355, 129

Seljak U. et al., 2005, Phys. Rev. D, 71, 043511

Sheldon E. S. et al., 2004, AJ, 127, 2544

Silk J., Rees M. J., 1998, A&A, 331, L1

Smith D. R., Bernstein G. M., Fischer P., Jarvis M., 2001, ApJ, 551, 643

Smith J. A. et al., 2002, AJ, 123, 2121

Stoughton C. et al., 2002, AJ, 123, 485

Strateva I. et al., 2001, AJ, 122, 1861

Strauss M. A. et al., 2002, AJ, 124, 1810

Tasitsiomi A., Kravtsov A. V., Wechsler R. H., Primack J. R., 2004, ApJ, 614, 533

Tegmark M. et al., 2004, ApJ, 606, 702

Tremonti C. A. et al., 2004, ApJ, 613, 898

Tucker D. et al., 2005, AJ, submitted

Tyson J. A., Valdes F., Jarvis J. F., Mills A. P., 1984, ApJ, 281, L59

Vale A., Ostriker J. P., 2004, MNRAS, 353, 189

van den Bosch F. C., Yang X., Mo H. J., 2003, MNRAS, 340, 771

van den Bosch F., Yang X., Mo H. J., 2004, Baryons in Dark Matter Halos. SISSA, Novigrad

van den Bosch F. C., Yang X., Mo H. J., Norberg P., 2005, MNRAS, 356, 1233

Weinberg D. H., Davé R., Katz N., Hernquist L., 2004, ApJ, 601, 1

Yang X. H., Mo H. J., Kauffmann G., Chu Y. Q., 2003, MNRAS, 339, 387

York D. G. et al., 2000, AJ, 120, 1579

Zehavi I. et al., 2005, ApJ, 630, 1

Zheng Z. et al., 2005, ApJ, 633, 791

This paper has been typeset from a TeX/LaTeX file prepared by the author.